Performance Analysis of Multi-Dimensional ESPRIT-Type Algorithms for Arbitrary and Strictly Non-Circular Sources With Spatial Smoothing

Jens Steinwandt, *Student Member, IEEE*, Florian Roemer, *Senior Member, IEEE*, Martin Haardt, *Senior Member, IEEE*, and Giovanni Del Galdo, *Member, IEEE*

***Abstract*—Spatial smoothing is a widely used preprocessing scheme to improve the performance of high-resolution parameter estimation algorithms in case of coherent signals or if only a small number of snapshots is available. In this paper, we present a first-order performance analysis of the spatially smoothed versions of R-D Standard ESPRIT and R-D Unitary ESPRIT for sources with arbitrary signal constellations as well as R-D NC Standard ESPRIT and R-D NC Unitary ESPRIT for strictly second-order (SO) non-circular (NC) sources. The derived expressions are asymptotic in the effective signal-to-noise ratio (SNR), i.e., the approximations become exact for either high SNRs or a large sample size. Moreover, no assumptions on the noise statistics are required apart from a zero mean and finite SO moments. We show that both R-D NC ESPRIT-type algorithms with spatial smoothing perform asymptotically identical in the high effective SNR regime. Generally, the performance of spatial smoothing based algorithms depends on the number of subarrays, which is a design parameter that needs to be chosen beforehand. In order to gain more insights into the optimal choice of the number of subarrays, we simplify the derived analytical R-D mean square error (MSE) expressions for the special case of a single source. The obtained MSE expression explicitly depends on the number of subarrays in each dimension, which allows us to analytically find the optimal number of subarrays for spatial smoothing. Based on this result, we additionally derive the maximum asymptotic gain from spatial smoothing and compute the asymptotic efficiency for the single source case in closed-form. All the analytical results are verified by simulations.**

***Index Terms*—Spatial smoothing, ESPRIT, non-circular sources, performance analysis, DOA estimation.**

I. Introduction

THE problem of high-resolution parameter estimation from multi-dimensional (R-D) signals with $R \geq 1$ has long been a fundamental research area in the field of array signal processing. Estimating, for instance, the directions of arrival, directions of departures, frequencies, Doppler shifts, etc. is required in a wide range of applications including radar [2], sonar [3], channel sounding [4], [5], and wireless communications [6]. R-D ESPRIT-type parameter estimation algorithms [7] have attracted considerable attention due to their fully algebraic estimates and their low complexity. As a result of their growing popularity, their analytical performance assessment has also been of great research interest. Two fundamental performance analysis concepts for 1-D parameter estimation have been established in [8] and [9]. While [8] relies on the eigenvector distribution of the sample covariance matrix and is only asymptotic in the sample size N, the framework in [9] provides an explicit first-order approximation of the parameter estimation error based on the superposition of the signal component by a small noise perturbation. The latter is asymptotic in the effective signal-to-noise ratio (SNR), i.e., the results become accurate for either high SNRs or a large sample size. Therefore, [9] is more general than [8] as it is even valid for $N = 1$ if the SNR is sufficiently high. In [10] and [11], this performance analysis framework has been extended to R-D parameter estimation, where no assumptions on the noise statistics apart from a zero mean and finite second-order (SO) moments are required for the analytical mean square error (MSE) expressions.

Previous work has shown that taking advantage of the statistical properties of the observed signals, i.e., their strictly SO non-circular (NC) structure [12], helps to improve the performance of conventional parameter estimation algorithms [13]–[20]. Such NC signals result from real-valued modulation schemes including BPSK, PAM, ASK, Offset-QPSK (after a derotation), etc. They are used in, for instance, wireless communications, cognitive radio, GNSS satellite systems, radar, tracking, and channel sounding. Recently, a number of improved subspace-based parameter estimation schemes, e.g., NC MUSIC [13]–[15], NC Root-MUSIC [16], NC Standard ESPRIT [17], and NC Unitary ESPRIT [18], [19] have been developed. It has been demonstrated that exploiting the prior knowledge on the signals' strict non-circularity significantly improves the estimation accuracy and doubles the number of identifiable sources [19]. The analytical performance of the MUSIC and ESPRIT-based NC algorithms has been investigated in [13], [19], [20]. For the special case of a single source, it was shown in [10]

Manuscript received January 18, 2016; revised July 30, 2016 and November 2, 2016; accepted December 16, 2016. Date of publication January 16, 2017; date of current version February 22, 2017. The associate editor coordinating the review of this manuscript and approving it for publication was Prof. Amir Asif. This paper was presented in part at the *IEEE Int. Conf. on Acoustics, Speech, and Signal Processing*, Florence, Italy, May 2014 [1]. *(Corresponding author: Jens Steinwandt.)*

J. Steinwandt and M. Haardt, are with Ilmenau University of Technology, D-98684 Ilmenau, Germany (e-mail: jens.steinwandt@tu-ilmenau.de; martin.haardt@tu-ilmenau.de; website: http://www.tu-ilmenau.de/crl).

F. Roemer and G. Del Galdo are with Ilmenau University of Technology, D-98684 Ilmenau, Germany, and also with the the Fraunhofer Institute for Integrated Circuits IIS (e-mail: florian.roemer@tu-ilmenau.de; giovanni.delgaldo@tu-ilmenau.de; website: http://www.tu-ilmenau.de/dvt).

Color versions of one or more of the figures in this paper are available online at http://ieeexplore.ieee.org.

Digital Object Identifier 10.1109/TSP.2017.2652388

along with [19] that neither forward-backward averaging (FBA) nor NC preprocessing in combination with ESPRIT-type algorithms improve the asymptotic MSE. The more general case of coexisting circular and strictly non-circular signals has been considered in [21]–[23].

The aforementioned NC algorithms and the conventional methods are known to yield a high resolution even in the case of correlated sources. However, they fail when more than two signals[1] are coherent (fully correlated) or if $N = 1$, as both render the signal covariance matrix rank-deficient. In practice, coherent signals often occur in a multipath environment [25] and the single snapshot case is often encountered in, e.g., channel sounding [5], nested arrays [26], tracking [27]. Assuming a uniform array geometry, preprocessing via spatial smoothing [28]–[30] can be applied to estimate the parameters of coherent signals. Spatial smoothing decorrelates coherent signals by averaging the data received by a number of subarrays L. As the resulting estimation error depends on L, it is a design parameter that can be optimized to achieve the best estimation accuracy. Several performance analyses of parameter estimation schemes using spatial smoothing based on the framework [8], which is, however, only asymptotic in N, have been presented in [31]–[37]. While [31]–[33] consider spatially smoothed MUSIC-type algorithms, the references [34]–[36] study ESPRIT-type algorithms. In [37], a performance analysis for an interpolated spatial smoothing algorithm for non-uniform linear arrays was proposed. The special case of spatial smoothing for a single source was considered in [32], [33], and in [34] for harmonic retrieval. It was observed that in this case a gain from spatial smoothing can be achieved. However, these existing performance analysis results only concern the 1-D parameter estimation. Analytical expressions for R-D parameter estimation algorithms such as R-D Standard ESPRIT and R-D Unitary ESPRIT with spatial smoothing as well as their recently proposed NC-versions R-D NC Standard ESPRIT and R-D NC Unitary ESPRIT with spatial smoothing have not been reported in the literature.

Therefore, in this paper, we present a first-order performance analysis for the spatially smoothed versions of R-D Standard ESPRIT and R-D Unitary ESPRIT as well as R-D NC Standard ESPRIT and R-D NC Unitary ESPRIT. We adopt the more general framework in [9], which is asymptotic in the high effective SNR. We assume a uniform R-D array geometry and use least squares (LS) to solve the shift invariance equations. However, as LS and total least squares (TLS) have been shown to perform asymptotically identical [8], the results obtained for LS are also valid for TLS. The derived closed-form MSE expressions are explicit in the noise realizations such that apart from a zero mean and finite SO moments, no further assumptions on the noise statistics are required. We show that due to the NC preprocessing both R-D NC ESPRIT-type algorithms with spatial smoothing perform identical in the high effective SNR. Further insights into the dependence of the MSE expressions on the physical parameters are provided by the case study of a single source. In particular, we first show that R-D spatial smoothing improves the estimation accuracy and that all the considered spatial smoothing based R-D ESPRIT-type algorithms provide the same MSE result, i.e., asymptotically, no additional gain is obtained from FBA and NC preprocessing. Based on these results, we analytically find the optimal number of subarrays L that minimizes the MSE in each of the R dimensions, which extends the 1-D results in [31]–[37]. This enables us to compute the maximum asymptotic R-D spatial smoothing gain for a single source in closed-form. Additionally, we analytically compute the asymptotic efficiency of the spatial smoothing based algorithms for $R = 1$.

This paper is organized as follows: The R-D data model and the preprocessing for NC sources are introduced in Section II. Section III reviews R-D spatial smoothing for ESPRIT-type and NC ESPRIT-type algorithms. Their performance analysis is presented in Section IV and Section V before the special case of a single source is analyzed in Section VI. Section VII illustrates the numerical results, and concluding remarks are drawn in Section VIII.

Notation: We use lower-case bold-face letters for column vectors and upper-case bold-face letters for matrices. The superscripts $^{\mathrm{T}}$, *, $^{\mathrm{H}}$, $^{-1}$, $^{+}$ denote the transposition, complex conjugation, conjugate transposition, matrix inversion, and the Moore-Penrose pseudo inverse, respectively. The Kronecker product is denoted as $\otimes$ and the Khatri-Rao product (column-wise Kronecker product) as $\diamond$. The operator $\mathrm{vec}\{\boldsymbol{A}\}$ stacks the columns of the matrix into a large column vector, $\mathrm{diag}\{\boldsymbol{a}\}$ returns a diagonal matrix with the elements of $\boldsymbol{a}$ placed on its diagonal, and $\mathrm{blkdiag}\{\cdot\}$ creates a block diagonal matrix. The operator $\mathcal{O}\{\cdot\}$ denotes the highest order with respect to a parameter. The matrix $\boldsymbol{\Pi}_M$ is the $M \times M$ exchange matrix with ones on its anti-diagonal and zeros elsewhere and $\underline{\mathbf{1}}$ denotes the vector of ones. Moreover, $\mathrm{Re}\{\cdot\}$ and $\mathrm{Im}\{\cdot\}$ extract the real and imaginary part of a complex number and $\arg\{\cdot\}$ extracts its phase. Also, $\|\boldsymbol{x}\|_2$ represents the 2-norm of the vector $\boldsymbol{x}$, and $\mathbb{E}\{\cdot\}$ stands for the statistical expectation. Furthermore, we use the short hand notation

$$\sum_{\underline{\boldsymbol{\ell}}=\underline{\mathbf{1}}}^{\underline{\boldsymbol{L}}} x_{\underline{\boldsymbol{\ell}}} = \sum_{\ell_1=1}^{L_1} \sum_{\ell_2=1}^{L_2} \cdots \sum_{\ell_R=1}^{L_R} x_{\ell_1,\ldots,\ell_R}, \tag{1}$$

where $\underline{\boldsymbol{\ell}} = [\ell_1, \ldots, \ell_r, \ldots, \ell_R]$ and $\underline{\boldsymbol{L}} = [L_1, \ldots, L_r, \ldots, L_R]$ with $\ell_r = 1, \ldots, L_r, r = 1, \ldots, R$.

II. Data Model

In this section, we introduce the R-D data model for arbitrary signals followed by the NC data model for strictly non-circular signals.

A. Data Model for Arbitrary Signals

Suppose the measurement data is represented by N subsequent observations of a noise-corrupted superposition of d undamped exponentials sampled on a separable uniform R-D grid of size $M_1 \times \ldots \times M_R$ [7]. The t_n-th time snapshot of the R-D measurements can be modeled as

$$x_{m_1,\ldots,m_R}(t_n) = \sum_{i=1}^{d} s_i(t_n) \prod_{r=1}^{R} \mathrm{e}^{\mathrm{j}(m_r-1)\mu_i^{(r)}} + n_{m_1,\ldots,m_R}(t_n), \tag{2}$$

[1]Two coherent signals can be separated by FBA if the array phase reference is not located at the array centroid [24].

where $m_r = 1, \ldots, M_r$, $n = 1, \ldots, N$, and $s_i(t_n)$ represents the complex amplitude of the i-th undamped exponential at the time instant t_n. Furthermore, $\mu_i^{(r)}$ is the i-th spatial frequency in the r-th mode, $i = 1, \ldots, d, r = 1, \ldots, R$, and $n_{m_1,\ldots,m_R}(t_n)$ denotes the zero-mean additive noise component. In the context of array signal processing, each of the R-D exponentials represents a narrow-band planar wavefront from a stationary far-field source and the complex amplitudes $s_i(t_n)$ describe the source symbols. The goal is to estimate the $R{\cdot}d$ spatial frequencies $\boldsymbol{\mu}_i = [\mu_i^{(1)}, \ldots, \mu_i^{(R)}]^{\mathrm{T}}$ from (2). We assume that d is known or has been estimated beforehand.

In order to obtain a more compact formulation of (2), we form the measurement matrix $\boldsymbol{X} \in \mathbb{C}^{M \times N}$ with $M = \prod_{r=1}^{R} M_r$ by stacking the R spatial dimensions along the rows and aligning the N time snapshots as the columns. This way, $\boldsymbol{X}$ can be modeled as

$$\boldsymbol{X} = \boldsymbol{A}\boldsymbol{S} + \boldsymbol{N} \in \mathbb{C}^{M \times N}, \tag{3}$$

where $\boldsymbol{S} \in \mathbb{C}^{d \times N}$ represents the source symbol matrix, $\boldsymbol{N} \in \mathbb{C}^{M \times N}$ contains the noise samples, and $\boldsymbol{A} = [\boldsymbol{a}(\boldsymbol{\mu}_1), \ldots, \boldsymbol{a}(\boldsymbol{\mu}_d)] \in \mathbb{C}^{M \times d}$ is the array steering matrix. The latter consists of the array steering vectors $\boldsymbol{a}(\boldsymbol{\mu}_i)$ corresponding to the i-th spatial frequency, which are given by

$$\boldsymbol{a}(\boldsymbol{\mu}_i) = \boldsymbol{a}^{(1)}\left(\mu_i^{(1)}\right) \otimes \cdots \otimes \boldsymbol{a}^{(R)}\left(\mu_i^{(R)}\right) \in \mathbb{C}^{M \times 1}, \tag{4}$$

where $\boldsymbol{a}^{(r)}(\mu_i^{(r)}) \in \mathbb{C}^{M_r \times 1}$ is the array steering vector in the r-th mode. Alternatively, $\boldsymbol{A}$ can be expressed as

$$\boldsymbol{A} = \boldsymbol{A}^{(1)} \diamond \boldsymbol{A}^{(2)} \diamond \cdots \diamond \boldsymbol{A}^{(R)}, \tag{5}$$

where $\boldsymbol{A}^{(r)} = [\boldsymbol{a}^{(r)}(\mu_1^{(r)}), \ldots, \boldsymbol{a}^{(r)}(\mu_d^{(r)})] \in \mathbb{C}^{M_r \times d}$ represents the array steering matrix in the r-th mode. For an arbitrary phase reference along the r-th mode, $\boldsymbol{A}^{(r)}$ can be decomposed as [38] $\boldsymbol{A}^{(r)} = \bar{\boldsymbol{A}}^{(r)}\boldsymbol{\Delta}^{(r)}$, where $\bar{\boldsymbol{A}}^{(r)} = [\bar{\boldsymbol{a}}^{(r)}(\mu_1^{(r)}), \cdots, \bar{\boldsymbol{a}}^{(r)}(\mu_d^{(r)})] \in \mathbb{C}^{M_r \times d}$ satisfies $\bar{\boldsymbol{A}}^{(r)} = \boldsymbol{\Pi}_{M_r}\bar{\boldsymbol{A}}^{(r)^*}$ and contains the steering vectors $\bar{\boldsymbol{a}}^{(r)}(\mu_i^{(r)}), i = 1, \ldots, d$, whose phase reference is located at the centroid of the r-th mode, i.e.,

$$\bar{\boldsymbol{a}}^{(r)}(\mu_i^{(r)}) = \left[\mathrm{e}^{-\mathrm{j}\frac{(M_r-1)}{2}\mu_i^{(r)}}, \ \cdots, \ \mathrm{e}^{\mathrm{j}\frac{(M_r-1)}{2}\mu_i^{(r)}}\right] \in \mathbb{C}^{M_r \times 1}. \tag{6}$$

Furthermore, the diagonal matrix $\boldsymbol{\Delta}^{(r)} = \mathrm{diag}\{\mathrm{e}^{\mathrm{j}\delta^{(r)}\mu_i^{(r)}}\}_{i=1}^{d}$ defines the shifts of the phase reference $\delta^{(r)} \in \left[\frac{-(M_r-1)}{2}, \frac{(M_r-1)}{2}\right]$ for each $\mu_i^{(r)}$. If the actual phase reference is at the array centroid of the r-th mode, we have $\delta^{(r)} = 0$, $\boldsymbol{\Delta}^{(r)} = \boldsymbol{I}_d$, and consequently $\boldsymbol{A}^{(r)} = \bar{\boldsymbol{A}}^{(r)}$. Thus, we can rewrite $\boldsymbol{A}$ in (5) as [38] $\boldsymbol{A} = \bar{\boldsymbol{A}}\boldsymbol{\Delta}$, where $\bar{\boldsymbol{A}} = \bar{\boldsymbol{A}}^{(1)} \diamond \bar{\boldsymbol{A}}^{(2)} \diamond \cdots \diamond \bar{\boldsymbol{A}}^{(R)} \in \mathbb{C}^{M \times d}$ and $\boldsymbol{\Delta} = \boldsymbol{\Delta}^{(1)} \cdot \boldsymbol{\Delta}^{(2)} \cdot \ldots \cdot \boldsymbol{\Delta}^{(R)} = \mathrm{diag}\{\mathrm{e}^{\mathrm{j}\delta_i}\}_{i=1}^{d} \in \mathbb{C}^{d \times d}$ with $\delta_i = \sum_{r=1}^{R} \delta^{(r)}\mu_i^{(r)}$. Again, if $\delta^{(r)} = 0, r = 1, \ldots, R$, we have $\boldsymbol{A} = \bar{\boldsymbol{A}}$. Using these relations, we obtain the model

$$\boldsymbol{X} = \bar{\boldsymbol{A}}\boldsymbol{\Delta}\boldsymbol{S} + \boldsymbol{N} = \bar{\boldsymbol{A}}\bar{\boldsymbol{S}} + \boldsymbol{N} \in \mathbb{C}^{M \times N}. \tag{7}$$

Due to the assumption that the R-D sampling grid is uniform, the array steering matrix $\boldsymbol{A}$ satisfies the shift invariance equation given by

$$\tilde{\boldsymbol{J}}_1^{(r)}\bar{\boldsymbol{A}}\boldsymbol{\Phi}^{(r)} = \tilde{\boldsymbol{J}}_2^{(r)}\bar{\boldsymbol{A}}, \quad r = 1, \ldots, R, \tag{8}$$

where $\tilde{\boldsymbol{J}}_1^{(r)}$ and $\tilde{\boldsymbol{J}}_2^{(r)} \in \mathbb{R}^{\frac{M}{M_r}(M_r-1) \times M}$ are the effective R-D selection matrices, which select $M_r - 1$ elements (maximum overlap) for the first and the second subarray in the r-th mode, respectively. They are compactly defined as $\tilde{\boldsymbol{J}}_k^{(r)} = \boldsymbol{I}_{\prod_{l=1}^{r-1} M_l} \otimes \boldsymbol{J}_k^{(r)} \otimes \boldsymbol{I}_{\prod_{l=r+1}^{R} M_l}$ for $k = 1, 2$, where $\boldsymbol{J}_k^{(r)} \in \mathbb{R}^{(M_r-1) \times M_r}$ are the r-mode selection matrices for the first and second subarray [7]. The diagonal matrix $\boldsymbol{\Phi}^{(r)} = \mathrm{diag}\{\mathrm{e}^{\mathrm{j}\mu_i^{(r)}}\}_{i=1}^{d} \in \mathbb{C}^{d \times d}$ contains the spatial frequencies in the r-th mode to be estimated.

B. Preprocessing for Strictly Non-Circular Signals

A zero-mean complex random variable $Z = X + \mathrm{j}Y$ is said to be SO non-circular if $\mathbb{E}\{Z^2\} \neq 0$ holds, which implies that its real and its imaginary part are correlated. The degree of non-circularity is usually defined by the non-circularity coefficient [12]

$$\kappa = \frac{\mathbb{E}\{Z^2\}}{\mathbb{E}\{|Z|^2\}} = |\kappa|\,\mathrm{e}^{\mathrm{j}\psi}, \quad 0 \leq |\kappa| \leq 1. \tag{9}$$

Random variables that satisfy $|\kappa| = 0$ or $0 < |\kappa| < 1$ are called circularly symmetric or weak-sense SO non-circular, respectively. The case $|\kappa| = 1$ describes a strictly SO non-circular (also referred to as rectilinear) random variable. The latter, which is considered in this work, implies a linear dependence between the real and the imaginary part of Z. Thus, Z can be represented as a real-valued random variable W which is rotated by a deterministic complex phase term $\mathrm{e}^{\mathrm{j}\varphi}$, i.e., $Z = W \cdot \mathrm{e}^{\mathrm{j}\varphi}$.

In a communication system, the case of strictly SO non-circular signals presumes that the sources transmit signals with real-valued constellations (BPSK, ASK, Offset-QPSK after a derotation, etc.). Due to the distinct transmission delays of the signals received from different sources, the symbol amplitudes at the receiver lie on lines with different phase rotations in the complex plane. Therefore, the symbol matrix $\boldsymbol{S}$ in (3) can be decomposed as [19] $\boldsymbol{S} = \boldsymbol{\Psi}\boldsymbol{S}_0$, where $\boldsymbol{S}_0 \in \mathbb{R}^{d \times N}$ is a real-valued symbol matrix and $\boldsymbol{\Psi} = \mathrm{diag}\{\mathrm{e}^{\mathrm{j}\varphi_i}\}_{i=1}^{d}$ contains the stationary complex phase shifts on its diagonal that are usually different for each source. Then, $\bar{\boldsymbol{S}}$ in (7) is given by $\bar{\boldsymbol{S}} = \boldsymbol{\Delta}\boldsymbol{\Psi}\boldsymbol{S}_0 = \boldsymbol{\Xi}\boldsymbol{S}_0$, where we have defined $\boldsymbol{\Xi} = \boldsymbol{\Delta}\boldsymbol{\Psi} = \mathrm{diag}\left\{\mathrm{e}^{\mathrm{j}(\varphi_i+\delta_i)}\right\}_{i=1}^{d}$.

In order to take advantage of the strict non-circularity of the signals, we apply a preprocessing scheme to (3) and define the augmented measurement matrix $\boldsymbol{X}^{(\mathrm{nc})} \in \mathbb{C}^{2M \times N}$ as [19]

$$\begin{aligned}\boldsymbol{X}^{(\mathrm{nc})} &= \begin{bmatrix}\boldsymbol{X} \\ \boldsymbol{\Pi}_M\boldsymbol{X}^*\end{bmatrix} = \begin{bmatrix}\bar{\boldsymbol{A}} \\ \bar{\boldsymbol{A}}\boldsymbol{\Xi}^*\boldsymbol{\Xi}^*\end{bmatrix}\bar{\boldsymbol{S}} + \begin{bmatrix}\boldsymbol{N} \\ \boldsymbol{\Pi}_M\boldsymbol{N}^*\end{bmatrix} \\ &= \bar{\boldsymbol{A}}^{(\mathrm{nc})}\bar{\boldsymbol{S}} + \boldsymbol{N}^{(\mathrm{nc})},\end{aligned} \tag{10}$$

where we have used the property $\boldsymbol{\Pi}_M\bar{\boldsymbol{A}}^* = \bar{\boldsymbol{A}}$. Moreover, $\bar{\boldsymbol{A}}^{(\mathrm{nc})} \in \mathbb{C}^{2M \times d}$ and $\boldsymbol{N}^{(\mathrm{nc})} \in \mathbb{C}^{2M \times N}$ are the augmented array steering matrix and the augmented noise matrix, respectively.

It was shown in [19] that if the array steering matrix $\bar{\boldsymbol{A}}$ is shift-invariant (8), then $\bar{\boldsymbol{A}}^{(\mathrm{nc})}$ is also shift-invariant and satisfies

$$\tilde{\boldsymbol{J}}_1^{(\mathrm{nc})(r)}\bar{\boldsymbol{A}}^{(\mathrm{nc})}\boldsymbol{\Phi}^{(r)} = \tilde{\boldsymbol{J}}_2^{(\mathrm{nc})(r)}\bar{\boldsymbol{A}}^{(\mathrm{nc})}, \quad r = 1, \ldots, R, \tag{11}$$

where $\tilde{\boldsymbol{J}}_k^{(\mathrm{nc})(r)} = \boldsymbol{I}_{\prod_{l=1}^{r-1} M_l} \otimes \boldsymbol{J}_k^{(\mathrm{nc})(r)} \otimes \boldsymbol{I}_{\prod_{l=r+1}^{R} M_l}$ and $\boldsymbol{J}_k^{(\mathrm{nc})(r)} = \boldsymbol{I}_2 \otimes \boldsymbol{J}_k^{(r)}, k = 1, 2$. Note that the extended dimensions of

$\bar{\boldsymbol{A}}^{(\mathrm{nc})}$ can be interpreted as a virtual doubling of the number of sensors, which leads to a lower estimation error and doubles the number of resolvable sources [19].

III. R-D Spatial Smoothing

In this section, we first apply R-D spatial smoothing to the data model for arbitrary signals in (3) before considering the data model for strictly non-circular sources in (10).

A. R-D Spatial Smoothing for Signals with Arbitrary Signal Constellations

In the case of coherent signals (fully correlated), or for a single snapshot $N = 1$, the symbol matrix $\bar{\boldsymbol{S}}$ becomes row rank-deficient, i.e., $\mathrm{rank}\{\bar{\boldsymbol{S}}\} < d$. If only two signals are coherent, forward-backward averaging (FBA) [30] can separate these signals if the corresponding diagonal elements of $\boldsymbol{\Delta}$ are distinct [24], i.e., the phase reference is not at the array centroid. For more than two coherent signals, however, the conventional subspace-based parameter estimators fail to estimate the directions of the coherent signals. In case of a uniform array geometry, spatial smoothing preprocessing can be applied to restore the full row rank d of $\bar{\boldsymbol{S}}$ albeit reducing the effective array aperture.

In order to perform R-D spatial smoothing, we apply 1-D spatial smoothing to each of the R dimensions independently [7]. To this end, the M_r uniform sampling grid points in the r-th dimension are divided into L_r maximally overlapping subarrays, each containing $M_{\mathrm{sub}_r} = M_r - L_r + 1$ elements. The corresponding $M_{\mathrm{sub}_r} \times M_r$ selection matrix for the ℓ_r-th subarray, $1 \le \ell_r \le L_r$ for $1 \le r \le R$, is defined as

$$\boldsymbol{J}_{\ell_r}^{(M_r)} = \left[\, \boldsymbol{0}_{M_{\mathrm{sub}_r} \times (\ell_r - 1)},\ \boldsymbol{I}_{M_{\mathrm{sub}_r}},\ \boldsymbol{0}_{M_{\mathrm{sub}_r} \times (L_r - \ell_r)} \,\right]. \quad (12)$$

Next, we define the $L = \prod_{r=1}^{R} L_r$ multi-dimensional selection matrices

$$\begin{aligned} \boldsymbol{J}_{\underline{\boldsymbol{\ell}}} &= \boldsymbol{J}_{\ell_1,\ldots,\ell_{R-1},\ell_R} \\ &= \boldsymbol{J}_{\ell_1}^{(M_1)} \otimes \cdots \otimes \boldsymbol{J}_{\ell_{R-1}}^{(M_{R-1})} \otimes \boldsymbol{J}_{\ell_R}^{(M_R)} \in \mathbb{R}^{M_{\mathrm{sub}} \times M} \end{aligned} \quad (13)$$

for $1 \le \ell_r \le L_r$ with $M_{\mathrm{sub}} = \prod_{r=1}^{R} M_{\mathrm{sub}_r}$. Then, the spatially smoothed data matrix $\boldsymbol{X}_{\mathrm{SS}} \in \mathbb{C}^{M_{\mathrm{sub}} \times NL}$, which is subsequently processed instead of $\boldsymbol{X}$, is given by

$$\begin{aligned} \boldsymbol{X}_{\mathrm{SS}} &= \left[\, \boldsymbol{J}_{1,\cdots,1,1}\boldsymbol{X},\ \boldsymbol{J}_{1,\cdots,1,2}\boldsymbol{X},\ \cdots,\ \boldsymbol{J}_{1,\cdots,1,L_R}\boldsymbol{X},\right. \\ &\qquad \left. \boldsymbol{J}_{1,\cdots,2,1}\boldsymbol{X},\ \cdots,\ \boldsymbol{J}_{L_1,\cdots,L_{R-1},L_R}\boldsymbol{X} \,\right] \\ &= \left[\, \boldsymbol{J}_{1,\cdots,1,1}\bar{\boldsymbol{A}}\bar{\boldsymbol{S}},\ \cdots,\ \boldsymbol{J}_{L_1,\cdots,L_{R-1},L_R}\bar{\boldsymbol{A}}\bar{\boldsymbol{S}} \,\right] \\ &\quad + \left[\, \boldsymbol{J}_{1,\cdots,1,1}\boldsymbol{N},\ \cdots,\ \boldsymbol{J}_{L_1,\cdots,L_{R-1},L_R}\boldsymbol{N} \,\right]. \end{aligned} \quad (14)$$

Note that by using (5) and (13), the array steering matrix of the ℓ-th subarray in all R modes can be expressed as

$$\begin{aligned} \boldsymbol{J}_{\ell_1,\ldots,\ell_{R-1},\ell_R}\bar{\boldsymbol{A}} &= \left(\boldsymbol{J}_{\ell_1}^{(M_1)}\bar{\boldsymbol{A}}^{(1)}\right) \diamond \cdots \diamond \left(\boldsymbol{J}_{\ell_R}^{(M_R)}\bar{\boldsymbol{A}}^{(R)}\right) \\ &= \left(\bar{\boldsymbol{A}}_1^{(1)}(\boldsymbol{\Phi}^{(1)})^{\ell_1 - 1}\right) \diamond \cdots \diamond \left(\bar{\boldsymbol{A}}_1^{(R)}(\boldsymbol{\Phi}^{(R)})^{\ell_R - 1}\right) \\ &= \bar{\boldsymbol{A}}_{\mathrm{SS}}\boldsymbol{\Phi}_{\ell_1,\ldots,\ell_{R-1},\ell_R}, \end{aligned} \quad (15)$$

where we have defined $\bar{\boldsymbol{A}}_1^{(r)} = \boldsymbol{J}_{1_r}^{(M_r)}\bar{\boldsymbol{A}}^{(r)} \in \mathbb{C}^{M_{\mathrm{sub}_r} \times d}$, $\bar{\boldsymbol{A}}_{\mathrm{SS}} = \bar{\boldsymbol{A}}_1^{(1)} \diamond \cdots \diamond \bar{\boldsymbol{A}}_1^{(R)} = \boldsymbol{J}_{1,\cdots,1,1}\bar{\boldsymbol{A}} \in \mathbb{C}^{M_{\mathrm{sub}} \times d}$, and

$$\boldsymbol{\Phi}_{\ell_1,\ldots,\ell_{R-1},\ell_R} = \prod_{r=1}^{R} (\boldsymbol{\Phi}^{(r)})^{\ell_r - 1}.$$

Consequently, we can rewrite (14) by applying (15) as

$$\boldsymbol{X}_{\mathrm{SS}} = \bar{\boldsymbol{A}}_{\mathrm{SS}}\boldsymbol{\Phi}\left(\boldsymbol{I}_L \otimes \bar{\boldsymbol{S}}\right) + \boldsymbol{N}_{\mathrm{SS}} = \boldsymbol{X}_{\mathrm{SS}_0} + \boldsymbol{N}_{\mathrm{SS}}, \quad (16)$$

where

$$\begin{aligned} \boldsymbol{\Phi} = [&\boldsymbol{\Phi}_{1,\ldots,1,1}, \cdots, \boldsymbol{\Phi}_{1,\ldots,1,L_R}, \boldsymbol{\Phi}_{1,\ldots,2,1}, \\ &\cdots, \boldsymbol{\Phi}_{L_1,\ldots,L_{R-1},L_R}] \in \mathbb{C}^{d \times Ld}, \end{aligned}$$

$\boldsymbol{X}_{\mathrm{SS}_0} \in \mathbb{C}^{M_{\mathrm{sub}} \times NL}$ is the noise-free spatially smoothed data matrix, and $\boldsymbol{N}_{\mathrm{SS}} \in \mathbb{C}^{M_{\mathrm{sub}} \times NL}$ is the spatially smoothed noise. Thus, spatial smoothing preprocessing reduces the array aperture to M_{sub} sensors and increases the number of snapshots by the factor L.

It is apparent that $\bar{\boldsymbol{A}}_{\mathrm{SS}}$ still satisfies the shift-invariance equation and we can write

$$\tilde{\boldsymbol{J}}_{\mathrm{SS}_1}^{(r)}\bar{\boldsymbol{A}}_{\mathrm{SS}}\boldsymbol{\Phi}^{(r)} = \tilde{\boldsymbol{J}}_{\mathrm{SS}_2}^{(r)}\bar{\boldsymbol{A}}_{\mathrm{SS}}, \quad r = 1, \ldots, R, \quad (17)$$

where $\tilde{\boldsymbol{J}}_{\mathrm{SS}_1}^{(r)}$ and $\tilde{\boldsymbol{J}}_{\mathrm{SS}_2}^{(r)} \in \mathbb{R}^{\frac{M_{\mathrm{sub}}}{M_{\mathrm{sub}_r}}(M_{\mathrm{sub}_r} - 1) \times M_{\mathrm{sub}}}$ are the R-D selection matrices that select $M_{\mathrm{sub}_r} - 1$ elements for the first and the second subarray in the r-th mode, respectively. They are compactly defined as $\tilde{\boldsymbol{J}}_{\mathrm{SS}_k}^{(r)} = \boldsymbol{I}_{\prod_{l=1}^{r-1} M_{\mathrm{sub}_l}} \otimes \boldsymbol{J}_{\mathrm{SS}_k}^{(r)} \otimes \boldsymbol{I}_{\prod_{l=r+1}^{R} M_{\mathrm{sub}_l}}$ for $k = 1, 2$, where $\boldsymbol{J}_{\mathrm{SS}_k}^{(r)} \in \mathbb{R}^{(M_{\mathrm{sub}_r} - 1) \times M_{\mathrm{sub}_r}}$ are the r-mode selection matrices for the first and second subarray. As (17) holds, the $R{\cdot}d$ spatial frequencies can be estimated by applying R-D ESPRIT-type algorithms to $\boldsymbol{X}_{\mathrm{SS}}$. In R-D Standard ESPRIT, the signal subspace $\hat{\boldsymbol{U}}_{\mathrm{SS}_s} \in \mathbb{C}^{M_{\mathrm{sub}} \times d}$ is estimated by computing the d dominant left singular vectors of $\boldsymbol{X}_{\mathrm{SS}}$. As $\bar{\boldsymbol{A}}_{\mathrm{SS}}$ and $\hat{\boldsymbol{U}}_{\mathrm{SS}_s}$ span approximately the same column space, a non-singular matrix $\boldsymbol{T} \in \mathbb{C}^{d \times d}$ can be found such that $\bar{\boldsymbol{A}}_{\mathrm{SS}} \approx \hat{\boldsymbol{U}}_{\mathrm{SS}_s}\boldsymbol{T}$. Using this relation, the overdetermined set of R shift invariance equations (17) can be expressed in terms of the estimated signal subspace, yielding

$$\tilde{\boldsymbol{J}}_{\mathrm{SS}_1}^{(r)}\hat{\boldsymbol{U}}_{\mathrm{SS}_s}\boldsymbol{\Gamma}^{(r)} \approx \tilde{\boldsymbol{J}}_{\mathrm{SS}_2}^{(r)}\hat{\boldsymbol{U}}_{\mathrm{SS}_s}, \quad r = 1, \ldots, R \quad (18)$$

with $\boldsymbol{\Gamma}^{(r)} \approx \boldsymbol{T}\boldsymbol{\Phi}^{(r)}\boldsymbol{T}^{-1}$. The R unknown matrices $\boldsymbol{\Gamma}^{(r)} \in \mathbb{C}^{d \times d}$ can be estimated, e.g., via least squares (LS), i.e.,

$$\hat{\boldsymbol{\Gamma}}^{(r)} \approx \left(\tilde{\boldsymbol{J}}_{\mathrm{SS}_1}^{(r)}\hat{\boldsymbol{U}}_{\mathrm{SS}_s}\right)^{+} \tilde{\boldsymbol{J}}_{\mathrm{SS}_2}^{(r)}\hat{\boldsymbol{U}}_{\mathrm{SS}_s}. \quad (19)$$

Finally, after solving (19) for $\hat{\boldsymbol{\Gamma}}^{(r)}$ in each mode independently, the correctly paired spatial frequency estimates are given by $\hat{\mu}_i^{(r)} = \arg\{\hat{\lambda}_i^{(r)}\}, i = 1, \ldots, d$. The eigenvalues $\hat{\lambda}_i^{(r)}$ of $\hat{\boldsymbol{\Gamma}}^{(r)}$ are obtained by performing a joint eigendecomposition across all R dimensions [39] or via the simultaneous Schur decomposition [7]. Alternatively, R-D Unitary ESPRIT [7] can be applied to estimate the $R{\cdot}d$ parameters, which is preferable due to its better performance at low SNRs and its real-valued implementation.

B. R-D Spatial Smoothing for Strictly Non-Circular Sources

If only NC sources are present, a modified spatial smoothing concept can be applied to the NC model in (10) [19], where we select $2M_{\mathrm{sub}}$ out of $2M$ virtual sensors. Thus, the L selection matrices in (13) are extended to

$$\boldsymbol{J}^{(\mathrm{nc})}_{\ell_1,\ldots,\ell_{R-1},\ell_R} = \boldsymbol{I}_2 \otimes \boldsymbol{J}_{\ell_1,\ldots,\ell_{R-1},\ell_R} \in \mathbb{R}^{2M_{\mathrm{sub}}\times 2M}. \quad (20)$$

The resulting spatially smoothed data matrix $\boldsymbol{X}^{(\mathrm{nc})}_{\mathrm{SS}}$ of size $2M_{\mathrm{sub}} \times NL$ is then given by

$$\boldsymbol{X}^{(\mathrm{nc})}_{\mathrm{SS}} = \Big[\boldsymbol{J}^{(\mathrm{nc})}_{1,\cdots,1,1}\boldsymbol{X}^{(\mathrm{nc})},\ \cdots,\ \boldsymbol{J}^{(\mathrm{nc})}_{1,\cdots,1,L_r}\boldsymbol{X}^{(\mathrm{nc})}, \boldsymbol{J}^{(\mathrm{nc})}_{1,\cdots,2,1}\boldsymbol{X}^{(\mathrm{nc})},\ \cdots,\ \boldsymbol{J}^{(\mathrm{nc})}_{L_1,\cdots,L_{R-1},L_R}\boldsymbol{X}^{(\mathrm{nc})} \Big]. \quad (21)$$

Following the lines of the previous subsection, we can compactly express (21) as

$$\begin{aligned}\boldsymbol{X}^{(\mathrm{nc})}_{\mathrm{SS}} &= \bar{\boldsymbol{A}}^{(\mathrm{nc})}_{\mathrm{SS}}\boldsymbol{\Phi}\left(\boldsymbol{I}_L \otimes \bar{\boldsymbol{S}}\right) + \boldsymbol{N}^{(\mathrm{nc})}_{\mathrm{SS}} \\ &= \boldsymbol{X}^{(\mathrm{nc})}_{\mathrm{SS}_0} + \boldsymbol{N}^{(\mathrm{nc})}_{\mathrm{SS}} \in \mathbb{C}^{2M_{\mathrm{sub}}\times NL}, \end{aligned} \quad (22)$$

where $\bar{\boldsymbol{A}}^{(\mathrm{nc})}_{\mathrm{SS}} = \boldsymbol{J}^{(\mathrm{nc})}_{1,\cdots,1,1}\bar{\boldsymbol{A}}^{(\mathrm{nc})} \in \mathbb{C}^{2M_{\mathrm{sub}}\times d}$ and $\boldsymbol{X}^{(\mathrm{nc})}_{\mathrm{SS}_0}$ is the unperturbed spatially smoothed NC data matrix. Note that spatial smoothing cannot be applied before $\boldsymbol{X}^{(\mathrm{nc})}$ is formed (10) as this would destroy the NC structure of the source signals.

As in the previous cases, $\bar{\boldsymbol{A}}^{(\mathrm{nc})}_{\mathrm{SS}}$ is shift-invariant and satisfies

$$\tilde{\boldsymbol{J}}^{(\mathrm{nc})(r)}_{\mathrm{SS}_1}\bar{\boldsymbol{A}}^{(\mathrm{nc})}_{\mathrm{SS}}\boldsymbol{\Phi}^{(r)} = \tilde{\boldsymbol{J}}^{(\mathrm{nc})(r)}_{\mathrm{SS}_2}\bar{\boldsymbol{A}}^{(\mathrm{nc})}_{\mathrm{SS}}, \quad r = 1,\ldots,R, \quad (23)$$

where $\tilde{\boldsymbol{J}}^{(\mathrm{nc})(r)}_{\mathrm{SS}_k} \in \mathbb{R}^{2\frac{M_{\mathrm{sub}}}{M_{\mathrm{sub}_r}}(M_{\mathrm{sub}_r}-1)\times 2M_{\mathrm{sub}}}, k = 1,2$ are the corresponding selection matrices that select $2(M_{\mathrm{sub}_r}-1)$ elements for the first and the second subarray in the r-th mode. They are defined as $\tilde{\boldsymbol{J}}^{(\mathrm{nc})(r)}_{\mathrm{SS}_k} = \boldsymbol{I}_{\prod_{l=1}^{r-1}M_l} \otimes \boldsymbol{J}^{(\mathrm{nc})(r)}_{\mathrm{SS}_k} \otimes \boldsymbol{I}_{\prod_{l=r+1}^{R}M_l}$, where $\boldsymbol{J}^{(\mathrm{nc})(r)}_{\mathrm{SS}_k} = \boldsymbol{I}_2 \otimes \boldsymbol{J}^{(r)}_{\mathrm{SS}_k} \in \mathbb{R}^{2(M_{\mathrm{sub}_r}-1)\times 2M_{\mathrm{sub}_r}}$ are the r-mode selection matrices for the first and second subarray. Again, R-D NC ESPRIT-type algorithms such as R-D NC Standard ESPRIT and R-D NC Unitary ESPRIT [19] can be used to estimate the $R{\cdot}d$ parameters.

IV. Performance of R-D ESPRIT-Type Algorithms With Spatial Smoothing

In this section, we present first-order error expansions of R-D Standard ESPRIT and R-D Unitary ESPRIT both with spatial smoothing. Moreover, we consider the special case of 2-D DOA estimation using 2-D Standard ESPRIT. The derived expressions rely on the data model (16) in Section III-A.

A. R-D Standard ESPRIT with Spatial Smoothing

For the perturbation analysis of the estimation error, we adopt the analytical framework proposed in [9] along with its extension in [11]. The authors of [9] assume a small additive noise perturbation and derive an explicit first-order error expansion of the subspace estimation error in terms of the noise $\boldsymbol{N}$, which is followed by a corresponding expression for the parameter estimation error $\Delta\mu_i$. As a follow-up, analytical expressions for the MSE that only require a zero mean and finite SO moments of the noise have been derived in [11]. From (16), it is clear that these assumptions are not violated by spatial smoothing such that [9] and [11] are still applicable for the performance analysis.

To derive the signal subspace estimation error for (16), we express the SVD of the noise-free spatially smoothed observations $\boldsymbol{X}_{\mathrm{SS}_0}$ as

$$\boldsymbol{X}_{\mathrm{SS}_0} = \begin{bmatrix}\boldsymbol{U}_{\mathrm{SS_s}} & \boldsymbol{U}_{\mathrm{SS_n}}\end{bmatrix}\begin{bmatrix}\boldsymbol{\Sigma}_{\mathrm{SS_s}} & \boldsymbol{0}\\ \boldsymbol{0} & \boldsymbol{0}\end{bmatrix}\begin{bmatrix}\boldsymbol{V}_{\mathrm{SS_s}} & \boldsymbol{V}_{\mathrm{SS_n}}\end{bmatrix}^{\mathrm{H}}, \quad (24)$$

where $\boldsymbol{U}_{\mathrm{SS_s}} \in \mathbb{C}^{M_{\mathrm{sub}}\times d}$, $\boldsymbol{U}_{\mathrm{SS_n}} \in \mathbb{C}^{M_{\mathrm{sub}}\times(NL-d)}$, and $\boldsymbol{V}_{\mathrm{SS_s}} \in \mathbb{C}^{NL\times d}$ span the signal subspace, the noise subspace, and the row space, respectively, and $\boldsymbol{\Sigma}_{\mathrm{SS_s}} \in \mathbb{R}^{d\times d}$ contains the non-zero singular values on its diagonal. Writing the perturbed signal subspace estimate $\hat{\boldsymbol{U}}_{\mathrm{SS_s}}$ computed from the SVD of $\boldsymbol{X}_{\mathrm{SS}}$ as $\hat{\boldsymbol{U}}_{\mathrm{SS_s}} = \boldsymbol{U}_{\mathrm{SS_s}} + \Delta\boldsymbol{U}_{\mathrm{SS_s}}$, where $\Delta\boldsymbol{U}_{\mathrm{SS_s}}$ denotes the signal subspace error, the first-order approximation using [9] is given by

$$\Delta\boldsymbol{U}_{\mathrm{SS_s}} = \boldsymbol{U}_{\mathrm{SS_n}}\boldsymbol{U}^{\mathrm{H}}_{\mathrm{SS_n}}\boldsymbol{N}_{\mathrm{SS}}\boldsymbol{V}_{\mathrm{SS_s}}\boldsymbol{\Sigma}^{-1}_{\mathrm{SS_s}} + \mathcal{O}\{\nu^2\}, \quad (25)$$

where $\nu = \|\boldsymbol{N}_{\mathrm{SS}}\|$, and $\|\cdot\|$ represents an arbitrary sub-multiplicative norm.[2] For the estimation error $\Delta\mu_i^{(r)}$ of the i-th spatial frequency in the r-th mode obtained by the LS solution, we have [9]

$$\Delta\mu_i^{(r)} = \mathrm{Im}\left\{\boldsymbol{p}_i^{\mathrm{T}}\left(\tilde{\boldsymbol{J}}^{(r)}_{\mathrm{SS}_1}\boldsymbol{U}_{\mathrm{SS_s}}\right)^{+}\left[\tilde{\boldsymbol{J}}^{(r)}_{\mathrm{SS}_2}/\lambda_i^{(r)} - \tilde{\boldsymbol{J}}^{(r)}_{\mathrm{SS}_1}\right]\Delta\boldsymbol{U}_{\mathrm{SS_s}}\boldsymbol{q}_i\right\} + \mathcal{O}\{\nu^2\}, \quad (26)$$

where $\lambda_i^{(r)} = \mathrm{e}^{\mathrm{j}\mu_i^{(r)}}$ is the i-th eigenvalue of $\boldsymbol{\Gamma}^{(r)}$, $\boldsymbol{q}_i$ represents the i-th eigenvector of $\boldsymbol{\Gamma}^{(r)}$ and the i-th column vector of the eigenvector matrix $\boldsymbol{Q}$, and $\boldsymbol{p}_i^{\mathrm{T}}$ is the i-th row vector of $\boldsymbol{P} = \boldsymbol{Q}^{-1}$. Hence, the eigendecomposition of $\boldsymbol{\Gamma}^{(r)}$ is given by $\boldsymbol{\Gamma}^{(r)} = \boldsymbol{Q}\boldsymbol{\Lambda}^{(r)}\boldsymbol{Q}^{-1}$, where $\boldsymbol{\Lambda}^{(r)}$ contains the eigenvalues $\lambda_i^{(r)}$ on its diagonal.

Finally, to compute the first-order MSE expression for R-D Standard ESPRIT with spatial smoothing, we extend the results in [11]. The MSE for the i-th spatial frequency in the r-th mode is given by

$$\mathbb{E}\left\{(\Delta\mu_i^{(r)})^2\right\} \approx \frac{1}{2}\left(\boldsymbol{r}^{(r)^{\mathrm{H}}}_{\mathrm{SS}_i}\boldsymbol{W}^{*}_{\mathrm{SS}}\boldsymbol{R}^{\mathrm{T}}_{\mathrm{SS}}\boldsymbol{W}^{\mathrm{T}}_{\mathrm{SS}}\boldsymbol{r}^{(r)}_{\mathrm{SS}_i} - \mathrm{Re}\left\{\boldsymbol{r}^{(r)^{\mathrm{T}}}_{\mathrm{SS}_i}\boldsymbol{W}_{\mathrm{SS}}\boldsymbol{C}^{\mathrm{T}}_{\mathrm{SS}}\boldsymbol{W}^{\mathrm{T}}_{\mathrm{SS}}\boldsymbol{r}^{(r)}_{\mathrm{SS}_i}\right\}\right), \quad (27)$$

where

$$\boldsymbol{r}^{(r)}_{\mathrm{SS}_i} = \boldsymbol{q}_i \otimes \left(\left[\left(\tilde{\boldsymbol{J}}^{(r)}_{\mathrm{SS}_1}\boldsymbol{U}_{\mathrm{SS_s}}\right)^{+}\left(\tilde{\boldsymbol{J}}^{(r)}_{\mathrm{SS}_2}/\lambda_i^{(r)} - \tilde{\boldsymbol{J}}^{(r)}_{\mathrm{SS}_1}\right)\right]^{\mathrm{T}}\boldsymbol{p}_i\right),$$

$$\boldsymbol{W}_{\mathrm{SS}} = \left(\boldsymbol{\Sigma}^{-1}_{\mathrm{SS_s}}\boldsymbol{V}^{\mathrm{T}}_{\mathrm{SS_s}}\right) \otimes \left(\boldsymbol{U}_{\mathrm{SS_n}}\boldsymbol{U}^{\mathrm{H}}_{\mathrm{SS_n}}\right) \in \mathbb{C}^{M_{\mathrm{sub}}d\times M_{\mathrm{sub}}NL}.$$

In order to compute (27), we require the covariance matrix $\boldsymbol{R}_{\mathrm{SS}} = \mathbb{E}\{\boldsymbol{n}_{\mathrm{SS}}\boldsymbol{n}^{\mathrm{H}}_{\mathrm{SS}}\} \in \mathbb{C}^{M_{\mathrm{sub}}NL\times M_{\mathrm{sub}}NL}$ and the pseudo-covariance matrix $\boldsymbol{C}_{\mathrm{SS}} = \mathbb{E}\{\boldsymbol{n}_{\mathrm{SS}}\boldsymbol{n}^{\mathrm{T}}_{\mathrm{SS}}\} \in \mathbb{C}^{M_{\mathrm{sub}}NL\times M_{\mathrm{sub}}NL}$ of the spatially smoothed noise $\boldsymbol{n}_{\mathrm{SS}} = \mathrm{vec}\{\boldsymbol{N}_{\mathrm{SS}}\} \in \mathbb{C}^{M_{\mathrm{sub}}NL\times 1}$. It is clear that the spatial smoothing preprocessing step modifies

[2] A matrix norm is called sub-multiplicative if $\|\boldsymbol{A}\cdot\boldsymbol{B}\| \le \|\boldsymbol{A}\|\cdot\|\boldsymbol{B}\|$ for arbitrary matrices $\boldsymbol{A}$ and $\boldsymbol{B}$.

the prior noise statistics, resulting in colored noise. However, in what follows, we analytically derive the SO noise statistics of the spatially smoothed noise. We first expand $\boldsymbol{n}_{\mathrm{SS}}$ as

$$\begin{aligned}\boldsymbol{n}_{\mathrm{SS}} &= \mathrm{vec}\left\{\left[\,\boldsymbol{J}_{1,\cdots,1,1}\boldsymbol{N},\ \cdots,\ \boldsymbol{J}_{L_1,\cdots,L_{R-1},L_R}\boldsymbol{N}\,\right]\right\} \\ &= \begin{bmatrix} (\boldsymbol{I}_N \otimes \boldsymbol{J}_{1,\cdots,1,1}) \\ \vdots \\ (\boldsymbol{I}_N \otimes \boldsymbol{J}_{L_1,\cdots,L_{R-1},L_R}) \end{bmatrix} \cdot \boldsymbol{n} = \boldsymbol{M}\cdot\boldsymbol{n}, \end{aligned} \tag{28}$$

where $\boldsymbol{M} \in \mathbb{R}^{M_{\mathrm{sub}}NL\times MN}$, $\boldsymbol{n} = \mathrm{vec}\{\boldsymbol{N}\} \in \mathbb{C}^{MN\times 1}$ is the unsmoothed noise component, and we have used the property $\mathrm{vec}\{\boldsymbol{AXB}\} = (\boldsymbol{B}^{\mathrm{T}}\otimes\boldsymbol{A})\,\mathrm{vec}\{\boldsymbol{X}\}$ for arbitrary matrices $\boldsymbol{A}$, $\boldsymbol{B}$, and $\boldsymbol{X}$ of appropriate sizes. Thus, the SO statistics of $\boldsymbol{n}_{\mathrm{SS}}$ can be expressed in terms of the covariance matrix $\boldsymbol{R}_{\mathrm{nn}} = \mathbb{E}\{\boldsymbol{n}\boldsymbol{n}^{\mathrm{H}}\} \in \mathbb{C}^{MN\times MN}$ and the pseudo-covariance matrix $\boldsymbol{C}_{\mathrm{nn}} = \mathbb{E}\{\boldsymbol{n}\boldsymbol{n}^{\mathrm{T}}\} \in \mathbb{C}^{MN\times MN}$ of $\boldsymbol{n}$. We obtain

$$\boldsymbol{R}_{\mathrm{SS}} = \boldsymbol{M}\boldsymbol{R}_{\mathrm{nn}}\boldsymbol{M}^{\mathrm{T}}, \quad \boldsymbol{C}_{\mathrm{SS}} = \boldsymbol{M}\boldsymbol{C}_{\mathrm{nn}}\boldsymbol{M}^{\mathrm{T}}. \tag{29}$$

B. R-D Unitary ESPRIT with Spatial Smoothing

It was shown in [11] that the asymptotic performance of R-D Unitary-ESPRIT is found once forward-backward-averaging (FBA) is taken into account. FBA is performed by replacing the spatially smoothed data matrix $\boldsymbol{X}_{\mathrm{SS}} \in \mathbb{C}^{M_{\mathrm{sub}}\times NL}$ by the column-augmented data matrix $\tilde{\boldsymbol{X}}_{\mathrm{SS}} \in \mathbb{C}^{M_{\mathrm{sub}}\times 2NL}$ defined by

$$\tilde{\boldsymbol{X}}_{\mathrm{SS}} = \left[\,\boldsymbol{X}_{\mathrm{SS}},\ \boldsymbol{\Pi}_{M_{\mathrm{sub}}}\boldsymbol{X}_{\mathrm{SS}}^{*}\boldsymbol{\Pi}_{NL}\,\right] = \tilde{\boldsymbol{X}}_{\mathrm{SS}_0} + \tilde{\boldsymbol{N}}_{\mathrm{SS}}, \tag{30}$$

where $\tilde{\boldsymbol{X}}_{\mathrm{SS}_0}$ is the noiseless FBA-processed spatially smoothed data matrix. Following the steps of the previous subsection, the first-order MSE expression for R-D Unitary ESPRIT with spatial smoothing for the i-th spatial frequency in the r-th mode is given by

$$\begin{aligned}\mathbb{E}\left\{(\Delta\mu_i^{(r)})^2\right\} \approx \frac{1}{2}\Big(&\tilde{\boldsymbol{r}}_{\mathrm{SS}_i}^{(r)\mathrm{H}}\tilde{\boldsymbol{W}}_{\mathrm{SS}}^{*}\tilde{\boldsymbol{R}}_{\mathrm{SS}}^{\mathrm{T}}\tilde{\boldsymbol{W}}_{\mathrm{SS}}^{\mathrm{T}}\tilde{\boldsymbol{r}}_{\mathrm{SS}_i}^{(r)} \\ &- \mathrm{Re}\left\{\tilde{\boldsymbol{r}}_{\mathrm{SS}_i}^{(r)\mathrm{T}}\tilde{\boldsymbol{W}}_{\mathrm{SS}}\tilde{\boldsymbol{C}}_{\mathrm{SS}}^{\mathrm{T}}\tilde{\boldsymbol{W}}_{\mathrm{SS}}^{\mathrm{T}}\tilde{\boldsymbol{r}}_{\mathrm{SS}_i}^{(r)}\right\}\Big)\end{aligned} \tag{31}$$

with

$$\tilde{\boldsymbol{r}}_{\mathrm{SS}_i}^{(r)} = \tilde{\boldsymbol{q}}_i \otimes \left(\left[\left(\tilde{\boldsymbol{J}}_{\mathrm{SS}_1}^{(r)}\tilde{\boldsymbol{U}}_{\mathrm{SS}_s}\right)^{+}\left(\tilde{\boldsymbol{J}}_{\mathrm{SS}_2}^{(r)}/\lambda_i^{(r)} - \tilde{\boldsymbol{J}}_{\mathrm{SS}_1}^{(r)}\right)\right]^{\mathrm{T}}\tilde{\boldsymbol{p}}_i\right),$$

$$\tilde{\boldsymbol{W}}_{\mathrm{SS}} = \left(\tilde{\boldsymbol{\Sigma}}_{\mathrm{SS}_s}^{-1}\tilde{\boldsymbol{V}}_{\mathrm{SS}_s}{}^{\mathrm{T}}\right)\otimes\left(\tilde{\boldsymbol{U}}_{\mathrm{SS}_n}\tilde{\boldsymbol{U}}_{\mathrm{SS}_n}^{\mathrm{H}}\right) \in \mathbb{C}^{M_{\mathrm{sub}}d\times 2M_{\mathrm{sub}}NL},$$

where we have replaced the noise-free subspaces of $\boldsymbol{X}_{\mathrm{SS}_0}$ in (27) by the corresponding subspaces of $\tilde{\boldsymbol{X}}_{\mathrm{SS}_0}$, and $\boldsymbol{p}_i$ and $\boldsymbol{q}_i$ by $\tilde{\boldsymbol{p}}_i$ and $\tilde{\boldsymbol{q}}_i$, respectively. It can be shown that $\tilde{\boldsymbol{n}}_{\mathrm{SS}} = \mathrm{vec}\{\tilde{\boldsymbol{N}}_{\mathrm{SS}}\} \in \mathbb{C}^{2M_{\mathrm{sub}}NL\times 1}$ is given by

$$\begin{aligned}\tilde{\boldsymbol{n}}_{\mathrm{SS}} &= \mathrm{vec}\left\{\left[\,\boldsymbol{N}_{\mathrm{SS}},\quad \boldsymbol{\Pi}_{M_{\mathrm{sub}}}\boldsymbol{N}_{\mathrm{SS}}^{*}\boldsymbol{\Pi}_{NL}\,\right]\right\} \\ &= \begin{bmatrix}\mathrm{vec}\{\boldsymbol{N}_{\mathrm{SS}}\} \\ \mathrm{vec}\{\boldsymbol{\Pi}_{M_{\mathrm{sub}}}\boldsymbol{N}_{\mathrm{SS}}^{*}\boldsymbol{\Pi}_{NL}\}\end{bmatrix} = \begin{bmatrix}\boldsymbol{n}_{\mathrm{SS}} \\ \boldsymbol{\Pi}_{M_{\mathrm{sub}}NL}\boldsymbol{n}_{\mathrm{SS}}^{*}\end{bmatrix}.\end{aligned} \tag{32}$$

Therefore, the expressions for $\tilde{\boldsymbol{R}}_{\mathrm{SS}} = \mathbb{E}\{\tilde{\boldsymbol{n}}_{\mathrm{SS}}\tilde{\boldsymbol{n}}_{\mathrm{SS}}^{\mathrm{H}}\} \in \mathbb{C}^{2M_{\mathrm{sub}}NL\times 2M_{\mathrm{sub}}NL}$ and $\tilde{\boldsymbol{C}}_{\mathrm{SS}} = \mathbb{E}\{\tilde{\boldsymbol{n}}_{\mathrm{SS}}\tilde{\boldsymbol{n}}_{\mathrm{SS}}^{\mathrm{T}}\} \in \mathbb{C}^{2M_{\mathrm{sub}}NL\times 2M_{\mathrm{sub}}NL}$ can be derived in terms of (29) as

$$\tilde{\boldsymbol{R}}_{\mathrm{SS}} = \boldsymbol{P}\begin{bmatrix}\boldsymbol{R}_{\mathrm{SS}} & \boldsymbol{C}_{\mathrm{SS}} \\ \boldsymbol{C}_{\mathrm{SS}}^{*} & \boldsymbol{R}_{\mathrm{SS}}^{*}\end{bmatrix}\boldsymbol{P}^{\mathrm{T}},\ \tilde{\boldsymbol{C}}_{\mathrm{SS}} = \boldsymbol{P}\begin{bmatrix}\boldsymbol{C}_{\mathrm{SS}} & \boldsymbol{R}_{\mathrm{SS}} \\ \boldsymbol{R}_{\mathrm{SS}}^{*} & \boldsymbol{C}_{\mathrm{SS}}^{*}\end{bmatrix}\boldsymbol{P}^{\mathrm{T}},$$

where $\boldsymbol{P} = \mathrm{blkdiag}\{\boldsymbol{I}_{M_{\mathrm{sub}}NL}, \boldsymbol{\Pi}_{M_{\mathrm{sub}}NL}\}$.

C. Special Case of 2-D DOA Estimation

In this section, we consider the practical task of 2-D DOA estimation using 2-D Standard ESPRIT with spatial smoothing, which is a special case of the generic R-D parameter model in (2). Using a 2-D rectangular array with half-wavelength element spacing, the relation between the two spatial frequencies $\mu_i^{(1)}$ and $\mu_i^{(2)}$ from (2) and the azimuth angle $\theta_i (-180^\circ < \theta_i \le 180^\circ)$ and the co-elevation angle $\phi_i (0^\circ \le \phi_i \le 90^\circ)$ of the i-th source is given by

$$\mu_i^{(1)} = \pi\cos\theta_i\sin\phi_i, \quad \mu_i^{(2)} = \pi\sin\theta_i\sin\phi_i. \tag{33}$$

The perturbed azimuth and co-elevation angles can be obtained via a first-order Taylor-series expansion of $\hat{\mu}_i^{(1)}$ and $\hat{\mu}_i^{(2)}$ as follows:

$$\hat{\mu}_i^{(1)} = \mu_i^{(1)} + \Delta\mu_i^{(1)} = \mu_i^{(1)} + \frac{\partial\mu_i^{(1)}}{\partial\theta_i}\Delta\theta_i + \frac{\partial\mu_i^{(1)}}{\partial\phi_i}\Delta\phi_i, \tag{34}$$

$$\hat{\mu}_i^{(2)} = \mu_i^{(2)} + \Delta\mu_i^{(2)} = \mu_i^{(2)} + \frac{\partial\mu_i^{(2)}}{\partial\theta_i}\Delta\theta_i + \frac{\partial\mu_i^{(2)}}{\partial\phi_i}\Delta\phi_i. \tag{35}$$

Thus, the respective first-order perturbation can be compactly expressed in matrix form as

$$\begin{bmatrix}\Delta\mu_i^{(1)} \\ \Delta\mu_i^{(2)}\end{bmatrix} = \begin{bmatrix}\frac{\partial\mu_i^{(1)}}{\partial\theta_i} & \frac{\partial\mu_i^{(1)}}{\partial\phi_i} \\ \frac{\partial\mu_i^{(2)}}{\partial\theta_i} & \frac{\partial\mu_i^{(2)}}{\partial\phi_i}\end{bmatrix}\begin{bmatrix}\Delta\theta_i \\ \Delta\phi_i\end{bmatrix}. \tag{36}$$

Solving (36) for the perturbations in the azimuth and co-elevation angles, yields

$$\Delta\theta_i = \tfrac{1}{\pi\sin\phi_i}\left(\cos\theta_i\cdot\Delta\mu_i^{(2)} - \sin\theta_i\cdot\Delta\mu_i^{(1)}\right), \tag{37}$$

$$\Delta\phi_i = \tfrac{1}{\pi\cos\phi_i}\left(\sin\theta_i\cdot\Delta\mu_i^{(2)} + \cos\theta_i\cdot\Delta\mu_i^{(1)}\right). \tag{38}$$

Then, the first-order MSE expression of (37) is given by

$$\begin{aligned}\mathbb{E}\left\{(\Delta\theta_i)^2\right\} \approx \left(\frac{1}{\pi\sin\phi_i}\right)^2\Big(&(\cos\theta_i)^2\,\mathbb{E}\{(\Delta\mu_i^{(2)})^2\} \\ &+ (\sin\theta_i)^2\,\mathbb{E}\{(\Delta\mu_i^{(1)})^2\} - 2\sin\theta_i\cos\theta_i\,\mathbb{E}\{\Delta\mu_i^{(1)}\Delta\mu_i^{(2)}\}\Big),\end{aligned}$$

where $\mathbb{E}\{(\Delta\mu_i^{(r)})^2\}, r = 1, 2$, of the i-th spatial frequency is given in (27) and $\mathbb{E}\{\Delta\mu_i^{(1)}\Delta\mu_i^{(2)}\}$ can be expressed according to [23] as

$$\begin{aligned}\mathbb{E}\left\{\Delta\mu_i^{(1)}\Delta\mu_i^{(2)}\right\} \approx \frac{1}{2}\Big(&\boldsymbol{r}_{\mathrm{SS}_i}^{(1)\mathrm{H}}\boldsymbol{W}_{\mathrm{SS}}^{*}\boldsymbol{R}_{\mathrm{SS}}^{\mathrm{T}}\boldsymbol{W}_{\mathrm{SS}}^{\mathrm{T}}\boldsymbol{r}_{\mathrm{SS}_i}^{(2)} \\ &- \mathrm{Re}\left\{\boldsymbol{r}_{\mathrm{SS}_i}^{(1)\mathrm{T}}\boldsymbol{W}_{\mathrm{SS}}\boldsymbol{C}_{\mathrm{SS}}^{\mathrm{T}}\boldsymbol{W}_{\mathrm{SS}}^{\mathrm{T}}\boldsymbol{r}_{\mathrm{SS}_i}^{(2)}\right\}\Big).\end{aligned} \tag{39}$$

In the same way, the first-order MSE expression of the co-elevation angle corresponding to (38) can be written as

$$\mathbb{E}\left\{(\Delta\phi_i)^2\right\} \approx \left(\frac{1}{\pi\cos\phi_i}\right)^2 \Big((\sin\theta_i)^2\,\mathbb{E}\big\{(\Delta\mu_i^{(2)})^2\big\} + (\cos\theta_i)^2\,\mathbb{E}\big\{(\Delta\mu_i^{(1)})^2\big\} + 2\sin\theta_i\cos\theta_i\,\mathbb{E}\big\{\Delta\mu_i^{(1)}\Delta\mu_i^{(2)}\big\}\Big).$$

V. Performance of R-D NC ESPRIT-Type Algorithms With Spatial Smoothing

In this section, we derive first-order analytical error expressions of R-D NC Standard ESPRIT and R-D NC Unitary ESPRIT for strictly non-circular sources both with spatial smoothing. As will be shown in Subsection V-B, the performance of both algorithms is asymptotically identical in the high effective SNR. Therefore, we first resort to the simpler derivation for the spatially smoothed R-D NC Standard ESPRIT algorithm and then show its equivalence to the spatially smoothed R-D NC Unitary ESPRIT algorithm. Our results are based on the data model (22) in Section III-B.

A. R-D NC Standard ESPRIT with Spatial Smoothing

In [19], we have shown that the framework of [9] is still applicable to the augmented measurement matrix $\boldsymbol{X}^{(\mathrm{nc})}$ (10) obtained by the preprocessing scheme for non-circular sources. From (22), it is apparent that adding spatial smoothing as a second preprocessing step does not violate the assumptions, such that the steps from Section IV-A can be applied to the spatially smoothed augmented data matrix $\boldsymbol{X}_{\mathrm{SS}}^{(\mathrm{nc})}$.

As a result, equivalently to (27), the first-order MSE expression for R-D NC Standard ESPRIT with spatial smoothing for the i-th spatial frequency in the r-th mode is given by

$$\mathbb{E}\left\{(\Delta\mu_i^{(r)})^2\right\} \approx \frac{1}{2}\left(\boldsymbol{r}_{\mathrm{SS}_i}^{(\mathrm{nc})(r)^{\mathrm{H}}}\boldsymbol{W}_{\mathrm{SS}}^{(\mathrm{nc})^*}\boldsymbol{R}_{\mathrm{SS}}^{(\mathrm{nc})^{\mathrm{T}}}\boldsymbol{W}_{\mathrm{SS}}^{(\mathrm{nc})^{\mathrm{T}}}\boldsymbol{r}_{\mathrm{SS}_i}^{(\mathrm{nc})(r)} - \mathrm{Re}\left\{\boldsymbol{r}_{\mathrm{SS}_i}^{(\mathrm{nc})(r)^{\mathrm{T}}}\boldsymbol{W}_{\mathrm{SS}}^{(\mathrm{nc})}\boldsymbol{C}_{\mathrm{SS}}^{(\mathrm{nc})^{\mathrm{T}}}\boldsymbol{W}_{\mathrm{SS}}^{(\mathrm{nc})^{\mathrm{T}}}\boldsymbol{r}_{\mathrm{SS}_i}^{(\mathrm{nc})(r)}\right\}\right), \quad (40)$$

where

$$\tilde{\boldsymbol{r}}_{\mathrm{SS}_i}^{(\mathrm{nc})(r)} = \boldsymbol{q}_i^{(\mathrm{nc})} \otimes \left(\left[\left(\tilde{\boldsymbol{J}}_{\mathrm{SS}_1}^{(\mathrm{nc})(r)}\boldsymbol{U}_{\mathrm{SS_s}}^{(\mathrm{nc})}\right)^+ \cdot \left(\tilde{\boldsymbol{J}}_{\mathrm{SS}_2}^{(\mathrm{nc})(r)}/\lambda_i^{(r)} - \tilde{\boldsymbol{J}}_{\mathrm{SS}_1}^{(\mathrm{nc})(r)}\right)\right]^{\mathrm{T}}\boldsymbol{p}_i^{(\mathrm{nc})}\right) \in \mathbb{C}^{2M_{\mathrm{sub}}d\times 1},$$

$$\boldsymbol{W}_{\mathrm{SS}}^{(\mathrm{nc})} = \left(\boldsymbol{\Sigma}_{\mathrm{SS_s}}^{(\mathrm{nc})^{-1}}\boldsymbol{V}_{\mathrm{SS_s}}^{(\mathrm{nc})^{\mathrm{T}}}\right)\otimes\left(\boldsymbol{U}_{\mathrm{SS_n}}^{(\mathrm{nc})}\boldsymbol{U}_{\mathrm{SS_n}}^{(\mathrm{nc})^{\mathrm{H}}}\right)\in\mathbb{C}^{2M_{\mathrm{sub}}d\times 2M_{\mathrm{sub}}NL},$$

where $\boldsymbol{p}_i^{(\mathrm{nc})}$ and $\boldsymbol{q}_i^{(\mathrm{nc})}$ replace $\boldsymbol{p}_i$ and $\boldsymbol{q}_i$, respectively. Moreover, we have used the corresponding subspaces of $\boldsymbol{X}_{\mathrm{SS}_0}^{(\mathrm{nc})}$ defined in (22) and the selection matrices $\tilde{\boldsymbol{J}}_{\mathrm{SS}_k}^{(\mathrm{nc})(r)}, k=1,2$, are given in (23).

The spatially smoothed augmented noise contribution $\boldsymbol{n}_{\mathrm{SS}}^{(\mathrm{nc})} = \mathrm{vec}\{\boldsymbol{N}_{\mathrm{SS}}^{(\mathrm{nc})}\} \in \mathbb{C}^{2M_{\mathrm{sub}}NL\times 1}$ can be expressed similarly to (28) as

$$\boldsymbol{n}_{\mathrm{SS}}^{(\mathrm{nc})} = \mathrm{vec}\left\{\left[\boldsymbol{J}_{1,\cdots,1,1}^{(\mathrm{nc})}\boldsymbol{N}^{(\mathrm{nc})},\ \cdots,\ \boldsymbol{J}_{L_1,\cdots,L_{R-1},L_R}^{(\mathrm{nc})}\boldsymbol{N}^{(\mathrm{nc})}\right]\right\} = \begin{bmatrix}(\boldsymbol{I}_N\otimes\boldsymbol{J}_{1,\cdots,1,1}^{(\mathrm{nc})})\\ \vdots \\ (\boldsymbol{I}_N\otimes\boldsymbol{J}_{L_1,\cdots,L_{R-1},L_R}^{(\mathrm{nc})})\end{bmatrix}\cdot\boldsymbol{n}^{(\mathrm{nc})} = \boldsymbol{M}^{(\mathrm{nc})}\cdot\boldsymbol{n}^{(\mathrm{nc})}, \quad (41)$$

where $\boldsymbol{M}^{(\mathrm{nc})}\in\mathbb{R}^{2M_{\mathrm{sub}}NL\times 2MN}$ and $\boldsymbol{n}^{(\mathrm{nc})} = \mathrm{vec}\{\boldsymbol{N}^{(\mathrm{nc})}\} \in \mathbb{C}^{2MN\times 1}$. Note that we have shown in [19] that $\boldsymbol{n}^{(\mathrm{nc})}$ can be represented as

$$\boldsymbol{n}^{(\mathrm{nc})} = \tilde{\boldsymbol{K}}\cdot\begin{bmatrix}\boldsymbol{n}\\ \boldsymbol{n}^*\end{bmatrix}, \quad (42)$$

where $\tilde{\boldsymbol{K}} = \boldsymbol{K}_{2M,N}^{\mathrm{T}}\cdot\mathrm{blkdiag}\{\boldsymbol{K}_{M,N}, \boldsymbol{K}_{M,N}\cdot(\boldsymbol{I}_N\otimes\boldsymbol{\Pi}_M)\}$ and $\boldsymbol{K}_{M,N}\in\mathbb{R}^{MN\times MN}$ is the commutation matrix that satisfies $\boldsymbol{K}_{M,N}\mathrm{vec}\{\boldsymbol{A}\} = \mathrm{vec}\{\boldsymbol{A}^{\mathrm{T}}\}$ for arbitrary matrices $\boldsymbol{A}\in\mathbb{C}^{M\times N}$ [40]. Then, $\boldsymbol{R}_{\mathrm{SS}}^{(\mathrm{nc})} = \mathbb{E}\{\boldsymbol{n}_{\mathrm{SS}}^{(\mathrm{nc})}\boldsymbol{n}_{\mathrm{SS}}^{(\mathrm{nc})^{\mathrm{H}}}\}\in\mathbb{C}^{2M_{\mathrm{sub}}NL\times 2M_{\mathrm{sub}}NL}$ and $\boldsymbol{C}_{\mathrm{SS}}^{(\mathrm{nc})} = \mathbb{E}\{\boldsymbol{n}_{\mathrm{SS}}^{(\mathrm{nc})}\boldsymbol{n}_{\mathrm{SS}}^{(\mathrm{nc})^{\mathrm{T}}}\}\in\mathbb{C}^{2M_{\mathrm{sub}}NL\times 2M_{\mathrm{sub}}NL}$ can be computed as

$$\boldsymbol{R}_{\mathrm{SS}}^{(\mathrm{nc})} = \boldsymbol{M}^{(\mathrm{nc})}\boldsymbol{R}_{\mathrm{nn}}^{(\mathrm{nc})}\boldsymbol{M}^{(\mathrm{nc})^{\mathrm{T}}}, \boldsymbol{C}_{\mathrm{SS}}^{(\mathrm{nc})} = \boldsymbol{M}^{(\mathrm{nc})}\boldsymbol{C}_{\mathrm{nn}}^{(\mathrm{nc})}\boldsymbol{M}^{(\mathrm{nc})^{\mathrm{T}}}, \quad (43)$$

where $\boldsymbol{R}_{\mathrm{nn}}^{(\mathrm{nc})}\in\mathbb{C}^{2MN\times 2MN}$ and $\boldsymbol{C}_{\mathrm{nn}}^{(\mathrm{nc})}\in\mathbb{C}^{2MN\times 2MN}$ are given by [19]

$$\boldsymbol{R}_{\mathrm{nn}}^{(\mathrm{nc})} = \mathbb{E}\left\{\boldsymbol{n}^{(\mathrm{nc})}\boldsymbol{n}^{(\mathrm{nc})^{\mathrm{H}}}\right\} = \tilde{\boldsymbol{K}}\begin{bmatrix}\boldsymbol{R}_{\mathrm{nn}} & \boldsymbol{C}_{\mathrm{nn}}\\ \boldsymbol{C}_{\mathrm{nn}}^* & \boldsymbol{R}_{\mathrm{nn}}^*\end{bmatrix}\tilde{\boldsymbol{K}}^{\mathrm{T}}, \quad (44)$$

$$\boldsymbol{C}_{\mathrm{nn}}^{(\mathrm{nc})} = \mathbb{E}\left\{\boldsymbol{n}^{(\mathrm{nc})}\boldsymbol{n}^{(\mathrm{nc})^{\mathrm{T}}}\right\} = \tilde{\boldsymbol{K}}\begin{bmatrix}\boldsymbol{C}_{\mathrm{nn}} & \boldsymbol{R}_{\mathrm{nn}}\\ \boldsymbol{R}_{\mathrm{nn}}^* & \boldsymbol{C}_{\mathrm{nn}}^*\end{bmatrix}\tilde{\boldsymbol{K}}^{\mathrm{T}}. \quad (45)$$

B. R-D NC Unitary ESPRIT with Spatial Smoothing

We have shown in [19] that R-D NC Standard ESPRIT and R-D NC Unitary ESPRIT both have the same asymptotic performance in the high effective SNR regime. It was established that applying FBA to the augmented matrix $\boldsymbol{X}^{(\mathrm{nc})}$ does not improve the signal subspace estimate and that the real-valued transformation has no effect on the asymptotic performance in the high effective SNR. In this subsection, we prove that these properties still hold when spatial smoothing is applied to both algorithms. To this end, we first investigate the effect of FBA and state the following theorem:

Theorem 1: Applying FBA to $\boldsymbol{X}_{\mathrm{SS}}^{(\mathrm{nc})}$ does not improve the signal subspace estimate.

Proof: The proof is given in Appendix A. ■

Next, we analyze the real-valued transformation as the second preprocessing step of R-D NC Unitary ESPRIT with spatial smoothing and formulate the theorem:

Theorem 2: The spatially smoothed R-D NC Unitary ESPRIT algorithm and the spatially smoothed R-D NC Standard ESPRIT algorithm with FBA preprocessing perform asymptotically identical in the high effective SNR.

Proof: The proof of this theorem follows the same steps as the one for the case without spatial smoothing considered in

[19]. This is due to the fact that spatial smoothing modifies the NC signal subspace of R-D NC Standard ESPRIT and R-D NC Unitary ESPRIT in the same way. ■

As a result of Theorem 1 and Theorem 2, we can conclude that the asymptotic performance of R-D NC Standard ESPRIT and R-D NC Unitary ESPRIT both with spatial smoothing is identical in the high effective SNR.

VI. Single Source Case

The derived analytical MSE expressions for the R-D ESPRIT-type methods with spatial smoothing are deterministic and formulated in terms of the subspaces of the noise-free observations. In [10] and [19], we have considered the special case of a single source for R-D ESPRIT-type methods without spatial smoothing to gain explicit insights into how the MSE expressions depend on the physical parameters, e.g., the number of sensors M, the sample size N, and the SNR. The knowledge of how the MSE expressions depend on these parameters can be of practical significance. For instance, this enables an objective comparison of different estimators or facilitates array design decisions on the value of M required to achieve a target MSE for a specific SNR. Note that establishing general MSE expressions for an arbitrary number of sources is challenging given the complex dependence of the subspaces on the physical parameters. For the single source case, it was proven in [10] and [19] that neither FBA nor NC preprocessing can improve the MSE. However, in this section, we show that a significant gain can be achieved for the MSE of R-D ESPRIT-type methods for a single source when spatial smoothing is applied. Assuming an R-D uniform sampling grid, i.e., a ULA in each mode, and circularly symmetric white noise, we simplify the derived MSE expressions in (27), (31), and (40) for this special case. The result depends on the number of subarrays L_r in the r-th mode as a design parameter, which we analytically compute in the R-D case by minimizing the MSE. It should be emphasized that these results for the special case $R = 1$ are in line with those derived in [32]–[34] for harmonic retrieval. Here, the R-D extension is provided. Based on our R-D results, we explicitly compute the asymptotic spatial smoothing gain for arbitrary R and the asymptotic efficiency for $R = 1$ in closed-form.

A. R-D ESPRIT-Type Algorithms with Spatial Smoothing

The final result for the simplified MSE expressions is summarized in the following theorem:

Theorem 3: For the case of an M-element R-D uniform sampling grid with an M_r-element ULA in the r-th mode, a single source ($d = 1$), and circularly symmetric white noise, the MSE in the r-th mode of R-D Standard ESPRIT and R-D Unitary ESPRIT with spatial smoothing as well as the MSE in the r-th mode of R-D NC Standard ESPRIT and R-D NC Unitary ESPRIT with spatial smoothing for a single source is given by $\mathrm{MSE}_{\mathrm{SS}}^{(r)} = \mathbb{E}\left\{(\Delta\mu^{(r)})^2\right\}$, yielding

$$\mathrm{MSE}_{\mathrm{SS}}^{(r)} \approx \begin{cases} \frac{1}{\hat{\rho}} \cdot \frac{1}{(M_r - L_r)^2 L_r} \cdot \prod_{\substack{p=1 \\ p \neq r}}^{R} \frac{c_p}{M_{\mathrm{sub}_p}^2 L_p^2} & \text{if } L_r \leq \frac{M_r}{2} \\ \frac{1}{\hat{\rho}} \cdot \frac{1}{(M_r - L_r) L_r^2} \cdot \prod_{\substack{p=1 \\ p \neq r}}^{R} \frac{c_p}{M_{\mathrm{sub}_p}^2 L_p^2} & \text{if } L_r > \frac{M_r}{2}, \end{cases} \tag{46}$$

where c_p is given as

$$c_p = \frac{1}{3} \cdot \Big(\min\{L_p, M_p - L_p\} + 1 \Big) \Big(\min\{L_p, M_p - L_p\} \cdot \big(2 \cdot \min\{L_p, M_p - L_p\} - 3 \cdot M_p - 2\big) + 6 \cdot M_{\mathrm{sub}_p} L_p \Big) - M_{\mathrm{sub}_p} L_p \tag{47}$$

and $\hat{\rho}$ represents the effective SNR $\hat{\rho} = N\hat{P}_{\mathrm{s}}/\sigma_{\mathrm{n}}^2$ with $\hat{P}_{\mathrm{s}}$ being the empirical source power given by $\hat{P}_{\mathrm{s}} = \|\boldsymbol{s}\|_2^2 / N$ and $\boldsymbol{s} \in \mathbb{C}^{N \times 1}$.

Proof: See Appendix B. ■

Note that (46) as a function of L_r is symmetric with respect to $L_r = M_r/2$. Moreover, (46) does not depend on the location of the phase reference $\delta^{(r)}$ of the array. In the special case of $R = 1$, where $M_r = M$ and $L_r = L$, the MSE in (46) simplifies to

$$\mathrm{MSE}_{\mathrm{SS}} \approx \begin{cases} \frac{1}{\hat{\rho}} \cdot \frac{1}{(M-L)^2 L} & \text{if } L \leq \frac{M}{2} \\ \frac{1}{\hat{\rho}} \cdot \frac{1}{(M-L) L^2} & \text{if } L > \frac{M}{2}. \end{cases} \tag{48}$$

Interestingly, we arrive at the same result for the MSE of all the considered spatially smoothed R-D ESPRIT-type algorithms for a single source, i.e., no additional gain from FBA or NC preprocessing can be achieved.

B. Optimal Number of Subarrays for Spatial Smoothing

In the MSE expression in (46), the number of subarrays L_r in each mode is a design parameter that can be optimized. Therefore, minimizing the MSE expression (46) with respect to L_r, yields[3]

$$L_r^{\mathrm{opt}} = \begin{cases} \frac{1}{3} \cdot M_r & \text{if } L_r \leq \frac{M_r}{2} \\ \frac{2}{3} \cdot M_r & \text{if } L_r > \frac{M_r}{2}, \end{cases} \tag{49}$$

where it is assumed that M_r is a multiple of 3. A short proof is provided in Appendix C. If M_r is not a multiple of 3, we round to the nearest integer. Then, L_r^{opt} for the case $L_r \leq \frac{M_r}{2}$, for instance, is given by

$$L_r^{\mathrm{opt}} = \begin{cases} \frac{1}{3} \cdot (M_r - 1) & \text{if } M_r \bmod 3 = 1 \\ \frac{1}{3} \cdot (M_r + 1) & \text{if } M_r \bmod 3 = 2. \end{cases} \tag{50}$$

It is worth highlighting that L_r^{opt} is independent of L_p and M_p for $p \neq r$, which is due to the separability of the array. Inserting L_r^{opt} from (49) and (50) into expression (46), we obtain $\mathrm{MSE}_{\mathrm{SS}_{\mathrm{opt}}}^{(r)} = \mathrm{MSE}_{\mathrm{SS}}^{(r)}(L_r^{\mathrm{opt}})$ as

$$\mathrm{MSE}_{\mathrm{SS}_{\mathrm{opt}}}^{(r)} \approx \begin{cases} \frac{1}{\hat{\rho}} \cdot \frac{27}{4} \cdot \frac{a}{M_r^3} & \text{if } M_r \bmod 3 = 0 \\ \frac{1}{\hat{\rho}} \cdot \frac{27}{4} \cdot \frac{a}{\left(M_r + \frac{1}{2}\right)^2 (M_r - 1)} & \text{if } M_r \bmod 3 = 1 \\ \frac{1}{\hat{\rho}} \cdot \frac{27}{4} \cdot \frac{a}{\left(M_r - \frac{1}{2}\right)^2 (M_r + 1)} & \text{if } M_r \bmod 3 = 2, \end{cases} \tag{51}$$

where $a = \prod_{\substack{p=1 \\ p \neq r}}^{R} \frac{c_p}{M_{\mathrm{sub}_p}^2 L_p^2}$. It is clear that the MSE for a fixed $\hat{\rho}$ is lowest when M_r is a multiple of 3. Again, for $R = 1$, these

[3] As (46) is symmetric with respect to $L_r = M_r/2$, we obtain two values for L_r^{opt} that both minimize the MSE and are equally valid.

results are in line with those derived in [32]–[34] for harmonic retrieval.

C. Asymptotic Spatial Smoothing Gain

Based on the result for L_r^{opt}, the maximum asymptotic gain obtained from spatial smoothing can be explicitly quantified. To this end, we contrast $\mathrm{MSE}_{\mathrm{SS}}^{(r)}(L_r^{\mathrm{opt}})$ from above with the result $\mathrm{MSE}^{(r)} = \frac{1}{\hat{\rho}} \cdot \frac{M_r}{M(M_r-1)^2}$ from [10] and [19] without spatial smoothing. The maximum asymptotic spatial smoothing gain in the r-th mode defined as $\eta_{\mathrm{SS}}^{(r)}(L_r^{\mathrm{opt}}) = \mathrm{MSE}^{(r)}/\mathrm{MSE}_{\mathrm{SS}}^{(r)}(L_r^{\mathrm{opt}})$ can be computed as

$$\eta_{\mathrm{SS}}^{(r)}(L_r^{\mathrm{opt}}) \approx \begin{cases} \frac{4}{27} \cdot \frac{M_r^4}{(M_r-1)^2} \cdot \frac{1}{Ma} & \text{if } M_r \bmod 3 = 0 \\ \frac{4}{27} \cdot \frac{M_r\left(M_r+\frac{1}{2}\right)^2}{(M_r-1)} \cdot \frac{1}{Ma} & \text{if } M_r \bmod 3 = 1 \\ \frac{4}{27} \cdot \frac{M_r(M_r-\frac{1}{2})^2(M_r+1)}{(M_r-1)^2 Ma} & \text{if } M_r \bmod 3 = 2. \end{cases} \quad (52)$$

D. Asymptotic Efficiency of 1-D ESPRIT-Type Algorithms with Spatial Smoothing

Furthermore, the optimal value for L_r^{opt} from Subsection VI-B allows to analytically compute the asymptotic efficiency of the considered R-D ESPRIT-type and R-D NC ESPRIT-type algorithms with spatial smoothing for a single source. To this end, we utilize the simplified single source expressions of the deterministic R-D Cramér-Rao bound (CRB) and R-D NC CRB in [10] and [19], respectively. As both expressions are identical, we here only state the conventional case from [10].

For the case of an M-element R-D uniform sampling grid with an M_r-element ULA in the r-th mode and a single source ($d = 1$), the deterministic R-D CRB can be simplified to [10]

$$\boldsymbol{C} = \mathrm{diag}\left\{\left[C^{(1)}, \ldots, C^{(R)}\right]^{\mathrm{T}}\right\}, \quad (53)$$

where $C^{(r)} = \frac{1}{\hat{\rho}} \cdot \frac{6}{M(M_r^2-1)}$. Using (46) and (53), the asymptotic efficiency $\eta^{(r)}(L_r^{\mathrm{opt}}) = \lim_{\hat{\rho}\to\infty} C^{(r)}/\mathrm{MSE}_{\mathrm{SS}}^{(r)}(L_r^{\mathrm{opt}})$ of the spatially smoothed versions of R-D Standard and R-D Unitary ESPRIT as well as R-D NC Standard and R-D NC Unitary ESPRIT can be computed in closed-form for arbitrary dimensions R. As an example, the asymptotic efficiency $\eta(L^{\mathrm{opt}})$ for $R = 1$ is given by

$$\eta(L^{\mathrm{opt}}) \approx \begin{cases} \frac{8}{9} \cdot \frac{M^2}{M^2-1} & \text{if } M \bmod 3 = 0 \\ \frac{8}{9} \cdot \frac{\left(M+\frac{1}{2}\right)^2}{M(M+1)} & \text{if } M \bmod 3 = 1 \\ \frac{8}{9} \cdot \frac{\left(M-\frac{1}{2}\right)^2}{M(M-1)} & \text{if } M \bmod 3 = 2. \end{cases} \quad (54)$$

It should be noted that η is only a function of the array geometry, i.e., the number of sensors M. Moreover, it is straightforward to see that the asymptotic efficiency is larger when M is a multiple of 3. As one of the main results from (54), we observe that $\lim_{M\to\infty} \eta(L^{\mathrm{opt}}) = 8/9$ for 1-D ESPRIT-type/NC ESPRIT-type algorithms with spatial smoothing. In contrast, it was shown in [10] and [19] that their counterparts without spatial smoothing become less efficient for increasing M, i.e., for $M \to \infty$, we have $\eta \to 0$. Consequently, spatial smoothing provides a significant gain for large M.

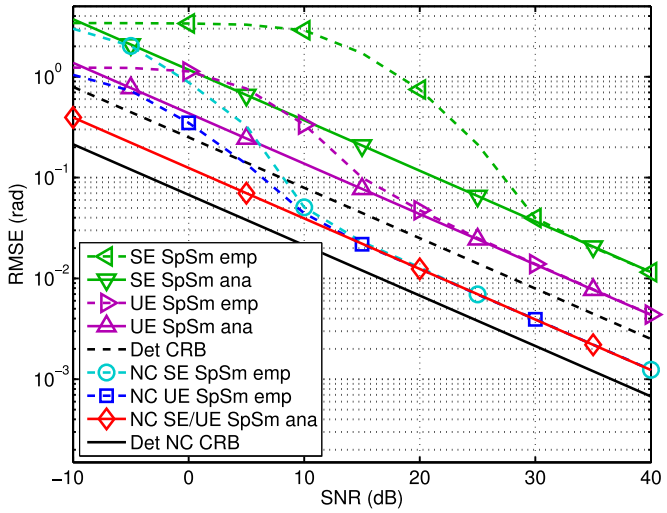

Fig. 1. RMSE versus SNR for a $6 \times 6 \times 6$ uniform cubic array ($R = 3$) and $N = 5$, $d = 2$ correlated sources ($\varrho = 0.9$) at $\mu_1^{(1)} = 0$, $\mu_2^{(1)} = 0.05$, $\mu_1^{(2)} = 0$, $\mu_2^{(2)} = 0.05$, $\mu_1^{(3)} = 0$, $\mu_2^{(3)} = 0.05$ with $\varphi_1 = 0$, $\varphi_2 = \pi/2$.

VII. Simulation Results

In this section, we present two sets of simulation results to assess the behavior of the derived performance analysis of ESPRIT-type algorithms based on spatial smoothing and to illustrate the analytical expressions for the single source case.

A. Performance Analysis

We first compare the square root of the analytical MSE expressions ("ana") in (27), (31), and (40) to the empirical ("emp") root mean square errors (RMSE)s of the spatially smoothed (SpSm) versions of R-D Standard ESPRIT (SE SpSm), R-D Unitary ESPRIT (UE SpSm) as well R-D NC Standard ESPRIT (NC SE SpSm) and R-D NC Unitary ESPRIT (NC UE SpSm). For all ESPRIT-type algorithms, LS is used to solve the shift invariance equations. We also include the deterministic Cramér-Rao bounds for arbitrary signals (Det CRB) and strictly SO non-circular sources (Det NC CRB) [38]. The total RMSE is defined as

$$\mathrm{RMSE} = \sqrt{\mathbb{E}\left\{\sum_{r=1}^{R}\sum_{i=1}^{d}\left(\mu_i^{(r)} - \hat{\mu}_i^{(r)}\right)^2\right\}}, \quad (55)$$

where $\hat{\mu}_i^{(r)}$ is the estimate of i-th spatial frequency in the r-th mode. It is assumed that a known number of signals with unit power impinge on uniform R-D array structures consisting of isotropic sensor elements with $\lambda/2$-interelement spacing in all dimensions. The phase reference is located at the array centroid. The symbols $\boldsymbol{S}_0$ are drawn from a real-valued Gaussian distribution and we assume zero-mean circularly symmetric white Gaussian noise. The curves are averaged over 5000 Monte Carlo trials.

In Fig. 1, we depict the total RMSE versus the SNR of $d = 2$ sources impinging on a $6 \times 6 \times 6$ uniform cubic array ($R = 3$) with $N = 5$. The sources are located at $\mu_1^{(1)} = 0$, $\mu_2^{(1)} = 0.05$, $\mu_1^{(2)} = 0$, $\mu_2^{(2)} = 0.05$, $\mu_1^{(3)} = 0$, and $\mu_2^{(3)} = 0.05$. They have a

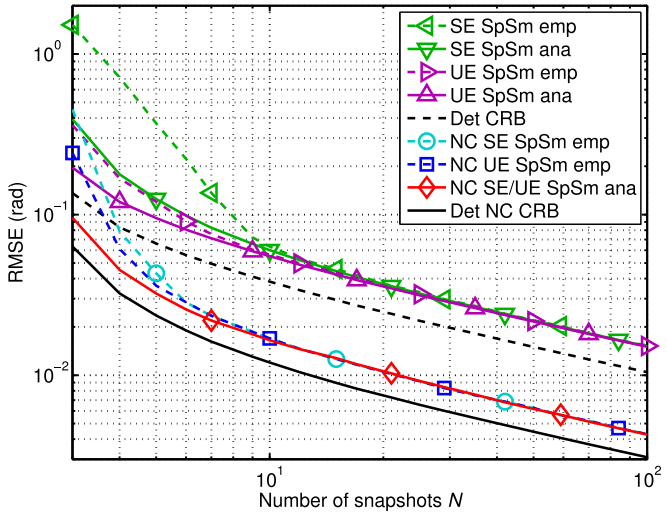

Fig. 2. RMSE versus N for a 6×6 URA ($R = 2$) and SNR $= 20$ dB, $d = 3$ uncorrelated sources ($\varrho = 0$) at $\mu_1^{(1)} = 0.25$, $\mu_2^{(1)} = 0.5$, $\mu_3^{(1)} = 0.75$, $\mu_1^{(2)} = 0.25$, $\mu_2^{(2)} = 0.5$, $\mu_3^{(2)} = 0.75$ with $\varphi_1 = 0$, $\varphi_2 = \pi/4$, $\varphi_3 = \pi/2$.

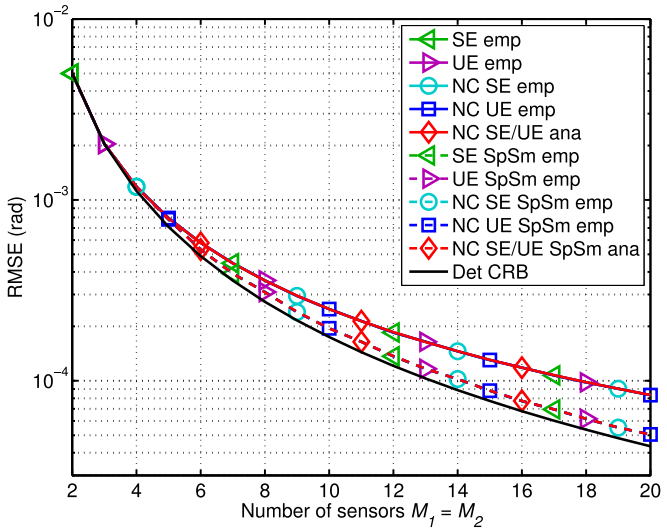

Fig. 3. RMSE versus $M_1 = M_2$ of a $M_1 \times M_2$ URA ($R = 2$) for a single source ($d = 1$) at $\mu^{(1)} = 0.1$, $\mu^{(2)} = 0.5$, and $\rho = 46$ dB ($P_s = 1$, $N = 4$, $\sigma_n^2 = 10^{-4}$).

pair-wise correlation of $\varrho = 0.9$ and their rotation phases contained in $\mathbf{\Psi}$ are given by $\varphi_1 = 0$ and $\varphi_2 = \pi/2$. For L_r, we choose $L_r^{\text{opt}} = M_r/3 = 2$ in each mode, i.e., we have divided the array into a total of $L = 8$ subarrays. Fig. 2 investigates the total RMSE versus the number of snapshots N for a 6×6 uniform rectangular array (URA) ($R = 2$), where the SNR is 20 dB and $L_r = L_r^{\text{opt}} = M_r/3 = 2$. We have $d = 3$ uncorrelated ($\varrho = 0$) sources at $\mu_1^{(1)} = 0.25$, $\mu_2^{(1)} = 0.5$, $\mu_3^{(1)} = 0.75$, $\mu_1^{(2)} = 0.25$, $\mu_2^{(2)} = 0.5$, and $\mu_3^{(2)} = 0.75$. The rotation phases are given by $\varphi_1 = 0$, $\varphi_2 = \pi/4$, and $\varphi_3 = \pi/2$.

It is apparent from Fig. 1 and Fig. 2 that the analytical results agree well with the empirical results for high effective SNRs, i.e., either high SNRs or a large sample size. Furthermore, NC SE SpSm and NC UE SpSm provide the lowest estimation errors and perform asymptotically identical in the high effective SNR regime. However, NC UE SpSm should be preferred due to its lower complexity and its better performance at low SNRs.

B. Analytical Results for a Single Source

In this subsection, the derived analytical results ("ana") in (51) and (54) for a single source ($d = 1$) are compared to their empirical versions. We also include the analytical and empirical single source results from [10] and [19] without spatial smoothing. The source is located at $\mu^{(1)} = 0.1$ and $\mu^{(2)} = 0.5$, however, its location has no impact on the MSE. The effective SNR is $\rho = 46$ dB with $P_s = 1$, $N = 4$, and $\sigma_n^2 = 10^{-4}$.

Fig. 3 illustrates the total RMSE using (51) as a function of the number of sensors $M_1 = M_2$ for a 2-D $M_1 \times M_2$ URA. We observe that the spatial smoothing based ESPRIT-type algorithms perform considerably closer to the CRB compared to the algorithms without spatial smoothing. Interestingly, there is no spatial smoothing gain up to $M_1 = M_2 = 4$ (a 4×4 URA). Then, as $M_1 = M_2$ grows, the spatial smoothing gain increases.

Fig. 4 presents the asymptotic efficiency (54) for $R = 1$ versus M of a ULA. The asymptotic efficiency for the non-spatial

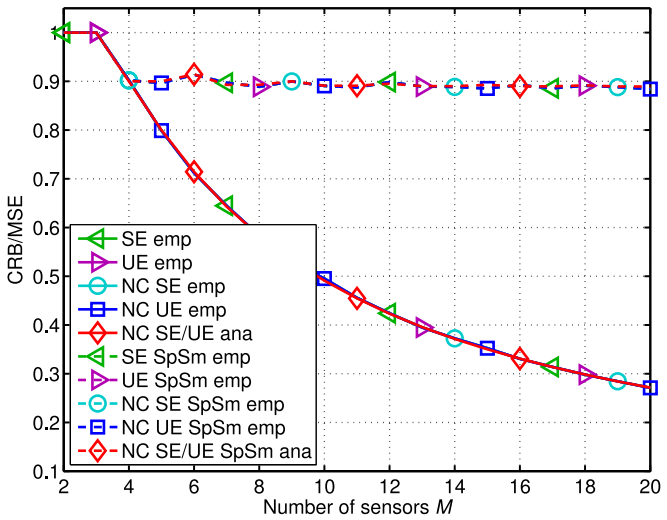

Fig. 4. Asymptotic efficiency versus M of a ULA ($R = 1$) for a single source ($d = 1$) at $\mu = 0$ and $\rho = 46$ dB ($P_s = 1$, $N = 4$, $\sigma_n^2 = 10^{-4}$).

smoothing case, i.e., $L = 1$, is given by $\eta(L = 1) = \frac{6(M-1)}{M(M+1)}$. It is clear from Fig. 4 that all the algorithms are asymptotically efficient for $M = 2$ and $M = 3$. As M increases further, the efficiency of the algorithms with spatial smoothing approaches the value $8/9$, while that of the non-spatial smoothing based algorithms becomes increasingly inefficient. Moreover, Fig. 4 confirms the observation from (54) that $\eta(L^{\text{opt}})$ is slightly higher for values of M that are multiples of 3.

VIII. Conclusion

This paper presents a first-order performance analysis of the spatially smoothed versions of R-D Standard ESPRIT and R-D Unitary ESPRIT for arbitrary sources as well as R-D NC Standard ESPRIT and R-D NC Unitary ESPRIT for strictly SO non-circular sources. The derived expressions are asymptotic

in the effective SNR and no assumptions on the noise statistics are required apart from a zero-mean and finite SO moments. We show that both spatially smoothed R-D NC ESPRIT-type algorithms perform asymptotically identical in the high effective SNR regime. As the performance generally depends on the number of subarrays, we have simplified the derived R-D MSE expressions for the special case of a single source, which allows to analytically compute the optimal number of subarrays for spatial smoothing. Additionally, we have derived the asymptotic spatial smoothing gain and calculated the asymptotic efficiency for the single source case. The analytical results are supported by simulations.

Appendix A Proof of Theorem 1

To show this result, we simply use the FBA-processed and spatially smoothed augmented measurement matrix

$$\tilde{\boldsymbol{X}}_{\mathrm{SS}}^{(\mathrm{nc})} = \left[\boldsymbol{X}_{\mathrm{SS}}^{(\mathrm{nc})},\ \boldsymbol{\Pi}_{2M_{\mathrm{sub}}} \boldsymbol{X}_{\mathrm{SS}}^{(\mathrm{nc})^*} \boldsymbol{\Pi}_{NL}\right] \in \mathbb{C}^{2M_{\mathrm{sub}} \times 2NL} \quad (56)$$

and compute the Gram matrix $\boldsymbol{G} = \tilde{\boldsymbol{X}}_{\mathrm{SS}}^{(\mathrm{nc})} \tilde{\boldsymbol{X}}_{\mathrm{SS}}^{(\mathrm{nc})^{\mathrm{H}}}$, which yields

$$\boldsymbol{G} = \boldsymbol{X}_{\mathrm{SS}}^{(\mathrm{nc})} \boldsymbol{X}_{\mathrm{SS}}^{(\mathrm{nc})^{\mathrm{H}}} + \boldsymbol{\Pi}_{2M_{\mathrm{sub}}} \boldsymbol{X}_{\mathrm{SS}}^{(\mathrm{nc})^*} \boldsymbol{X}_{\mathrm{SS}}^{(\mathrm{nc})^{\mathrm{T}}} \boldsymbol{\Pi}_{2M_{\mathrm{sub}}}. \quad (57)$$

Expanding the second term of (57) using (21), we obtain

$$\begin{aligned}
&\boldsymbol{\Pi}_{2M_{\mathrm{sub}}} \left(\sum_{\underline{\boldsymbol{\ell}}=\underline{\mathbf{1}}}^{\underline{\boldsymbol{L}}} \boldsymbol{J}_{\underline{\boldsymbol{\ell}}}^{(\mathrm{nc})} \boldsymbol{X}^{(\mathrm{nc})^*} \boldsymbol{X}^{(\mathrm{nc})^{\mathrm{T}}} \boldsymbol{J}_{\underline{\boldsymbol{\ell}}}^{(\mathrm{nc})^{\mathrm{T}}} \right) \boldsymbol{\Pi}_{2M_{\mathrm{sub}}} \\
&= \sum_{\underline{\boldsymbol{\ell}}=\underline{\mathbf{1}}}^{\underline{\boldsymbol{L}}} \begin{bmatrix} \boldsymbol{\Pi}_{M_{\mathrm{sub}}} \boldsymbol{J}_{\underline{\boldsymbol{\ell}}} \boldsymbol{\Pi}_M \boldsymbol{X} \boldsymbol{X}^{\mathrm{H}} \boldsymbol{\Pi}_M \boldsymbol{J}_{\underline{\boldsymbol{\ell}}}^{\mathrm{T}} \boldsymbol{\Pi}_{M_{\mathrm{sub}}} & \boldsymbol{\Pi}_{M_{\mathrm{sub}}} \boldsymbol{J}_{\underline{\boldsymbol{\ell}}} \boldsymbol{\Pi}_M \boldsymbol{X} \boldsymbol{X}^{\mathrm{T}} \boldsymbol{J}_{\underline{\boldsymbol{\ell}}}^{\mathrm{T}} \boldsymbol{\Pi}_{M_{\mathrm{sub}}} \\ \boldsymbol{\Pi}_{M_{\mathrm{sub}}} \boldsymbol{J}_{\underline{\boldsymbol{\ell}}} \boldsymbol{X}^* \boldsymbol{X}^{\mathrm{H}} \boldsymbol{\Pi}_M \boldsymbol{J}_{\underline{\boldsymbol{\ell}}}^{\mathrm{T}} \boldsymbol{\Pi}_{M_{\mathrm{sub}}} & \boldsymbol{\Pi}_{M_{\mathrm{sub}}} \boldsymbol{J}_{\underline{\boldsymbol{\ell}}} \boldsymbol{X}^* \boldsymbol{X}^{\mathrm{T}} \boldsymbol{J}_{\underline{\boldsymbol{\ell}}}^{\mathrm{T}} \boldsymbol{\Pi}_{M_{\mathrm{sub}}} \end{bmatrix}. \quad (58)
\end{aligned}$$

Next, we observe the symmetries $\boldsymbol{\Pi}_{M_{\mathrm{sub}}} \boldsymbol{J}_{\underline{\boldsymbol{\ell}}} \boldsymbol{\Pi}_M = \boldsymbol{J}_{\underline{\boldsymbol{L}}-\underline{\boldsymbol{\ell}}+\underline{\mathbf{1}}}$ and $\boldsymbol{\Pi}_{M_{\mathrm{sub}}} \boldsymbol{J}_{\underline{\boldsymbol{\ell}}} = \boldsymbol{J}_{\underline{\boldsymbol{L}}-\underline{\boldsymbol{\ell}}+\underline{\mathbf{1}}} \boldsymbol{\Pi}_M$. Hence, we perform a change of variables to $\underline{\boldsymbol{m}} = \underline{\boldsymbol{L}} - \underline{\boldsymbol{\ell}} + \underline{\mathbf{1}}$, which simplifies (58) to

$$\begin{aligned}
&\sum_{\underline{\boldsymbol{m}}=\underline{\mathbf{1}}}^{\underline{\boldsymbol{L}}} \begin{bmatrix} \boldsymbol{J}_{\underline{\boldsymbol{m}}} \boldsymbol{X} \boldsymbol{X}^{\mathrm{H}} \boldsymbol{J}_{\underline{\boldsymbol{m}}}^{\mathrm{T}} & \boldsymbol{J}_{\underline{\boldsymbol{m}}} \boldsymbol{X} \boldsymbol{X}^{\mathrm{T}} \boldsymbol{\Pi}_M \boldsymbol{J}_{\underline{\boldsymbol{m}}}^{\mathrm{T}} \\ \boldsymbol{J}_{\underline{\boldsymbol{m}}} \boldsymbol{\Pi}_M \boldsymbol{X}^* \boldsymbol{X}^{\mathrm{H}} \boldsymbol{J}_{\underline{\boldsymbol{m}}}^{\mathrm{T}} & \boldsymbol{J}_{\underline{\boldsymbol{m}}} \boldsymbol{\Pi}_M \boldsymbol{X}^* \boldsymbol{X}^{\mathrm{T}} \boldsymbol{\Pi}_M \boldsymbol{J}_{\underline{\boldsymbol{m}}}^{\mathrm{T}} \end{bmatrix} \\
&= \boldsymbol{X}_{\mathrm{SS}}^{(\mathrm{nc})} \boldsymbol{X}_{\mathrm{SS}}^{(\mathrm{nc})^{\mathrm{H}}}. \quad (59)
\end{aligned}$$

Replacing the second term of (57) by (59), we have $\boldsymbol{G} = 2 \cdot \boldsymbol{X}_{\mathrm{SS}}^{(\mathrm{nc})} \boldsymbol{X}_{\mathrm{SS}}^{(\mathrm{nc})^{\mathrm{H}}}$. Thus, the matrix $\boldsymbol{G}$ reduces to the scaled Gram matrix of $\boldsymbol{X}_{\mathrm{SS}}^{(\mathrm{nc})}$, i.e., the column space of $\boldsymbol{X}_{\mathrm{SS}}^{(\mathrm{nc})}$ is the same as the column space of the Gram matrix of $\boldsymbol{X}_{\mathrm{SS}}^{(\mathrm{nc})}$. Consequently, FBA has no effect on the column space of $\boldsymbol{X}_{\mathrm{SS}}^{(\mathrm{nc})}$. This completes the proof. ■

Appendix B Proof of Theorem 3

This theorem consists of several parts, which we address in separate subsections.

A. MSE for R-D Standard ESPRIT with Spatial Smoothing

We start the proof by simplifying the MSE expression for R-D Standard ESPRIT with spatial smoothing in (27) and for $d = 1$. In the single source case, the noise-free spatially smoothed measurement matrix $\boldsymbol{X}_{\mathrm{SS}_0} \in \mathbb{C}^{M_{\mathrm{sub}} \times NL}$ can be written as

$$\begin{aligned}
\boldsymbol{X}_{\mathrm{SS}_0} &= \bar{\boldsymbol{a}}_{\mathrm{SS}}(\boldsymbol{\mu}) \boldsymbol{\phi}^{\mathrm{T}} \left(\boldsymbol{I}_L \otimes \bar{\boldsymbol{s}}^{\mathrm{T}} \right) = \bar{\boldsymbol{a}}_{\mathrm{SS}}(\boldsymbol{\mu}) \boldsymbol{a}_L^{\mathrm{T}} \left(\boldsymbol{I}_L \otimes \bar{\boldsymbol{s}}^{\mathrm{T}} \right) \\
&= \bar{\boldsymbol{a}}_{\mathrm{SS}}(\boldsymbol{\mu}) \left(\boldsymbol{a}_L \otimes \bar{\boldsymbol{s}} \right)^{\mathrm{T}} = \bar{\boldsymbol{a}}_{\mathrm{SS}}(\boldsymbol{\mu}) \bar{\boldsymbol{s}}_L^{\mathrm{T}}, \quad (60)
\end{aligned}$$

where $\bar{\boldsymbol{a}}_{\mathrm{SS}}(\boldsymbol{\mu}) = \bar{\boldsymbol{a}}_1^{(1)}(\mu^{(1)}) \otimes \cdots \otimes \bar{\boldsymbol{a}}_1^{(R)}(\mu^{(R)}) \in \mathbb{C}^{M_{\mathrm{sub}} \times 1}$ is the spatially smoothed array steering vector in all R modes with $\bar{\boldsymbol{a}}_1^{(r)}(\mu^{(r)}) = \boldsymbol{J}_{1_r}^{(M_r)} \bar{\boldsymbol{a}}^{(r)}(\mu^{(r)}) \in \mathbb{C}^{M_{\mathrm{sub}_r} \times 1}, r = 1, \ldots, R$ and $\boldsymbol{\phi} = \boldsymbol{a}_L = \boldsymbol{a}_{L_1}^{(1)}(\mu^{(1)}) \otimes \cdots \otimes \boldsymbol{a}_{L_R}^{(R)}(\mu^{(R)}) \in \mathbb{C}^{L \times 1}$ with $\boldsymbol{a}_{L_r}^{(r)}(\mu^{(r)}) = [1, \mathrm{e}^{\mathrm{j}\mu^{(r)}}, \ldots, \mathrm{e}^{\mathrm{j}\mu^{(r)}(L_r-1)}]^{\mathrm{T}} \in \mathbb{C}^{L_r \times 1}$. Moreover, $\bar{\boldsymbol{s}} = \mathrm{e}^{\mathrm{j}\delta} \boldsymbol{s} \in \mathbb{C}^{N \times 1}$ with $\delta = \sum_{r=1}^{R} \delta^{(r)} \mu^{(r)}$ contains the source symbols with the empirical source power $\hat{P}_{\mathrm{s}} = \|\bar{\boldsymbol{s}}\|_2^2 / N$ and we have $\bar{\boldsymbol{s}}_L^{\mathrm{H}} \bar{\boldsymbol{s}}_L = NL\hat{P}_{\mathrm{s}}$. In what follows, we drop the dependence of $\bar{\boldsymbol{a}}_{\mathrm{SS}}(\boldsymbol{\mu})$ on $\boldsymbol{\mu}$ for notational convenience. For a ULA of isotropic elements in each of the R modes, $\bar{\boldsymbol{a}}^{(r)}$ is given by (6) and $\|\bar{\boldsymbol{a}}_{\mathrm{SS}}\|_2^2 = M_{\mathrm{sub}} = M - L + 1$. The selection matrices $\tilde{\boldsymbol{J}}_{\mathrm{SS}_1}^{(r)}$ and $\tilde{\boldsymbol{J}}_{\mathrm{SS}_2}^{(r)}$ are chosen as $\tilde{\boldsymbol{J}}_{\mathrm{SS}_1}^{(r)} = [\boldsymbol{I}_{M_{\mathrm{sub}_r}-1}, \boldsymbol{0}_{(M_{\mathrm{sub}_r}-1)\times 1}]$ and $\tilde{\boldsymbol{J}}_{\mathrm{SS}_2}^{(r)} = [\boldsymbol{0}_{(M_{\mathrm{sub}_r}-1)\times 1}, \boldsymbol{I}_{M_{\mathrm{sub}_r}-1}]$ for maximum overlap. Note that (60) is a rank-one matrix and we can directly determine the subspaces from the SVD as

$$\begin{aligned}
\boldsymbol{U}_{\mathrm{SS}_{\mathrm{s}}} &= \boldsymbol{u}_{\mathrm{SS}_{\mathrm{s}}} = \frac{\bar{\boldsymbol{a}}_{\mathrm{SS}}}{\|\bar{\boldsymbol{a}}_{\mathrm{SS}}\|_2} = \frac{\bar{\boldsymbol{a}}_{\mathrm{SS}}}{\sqrt{M_{\mathrm{sub}}}}, \\
\boldsymbol{\Sigma}_{\mathrm{SS}_{\mathrm{s}}} &= \sigma_{\mathrm{SS}_{\mathrm{s}}} = \sqrt{M_{\mathrm{sub}} NL\hat{P}_{\mathrm{s}}}, \\
\boldsymbol{V}_{\mathrm{SS}_{\mathrm{s}}} &= \boldsymbol{v}_{\mathrm{SS}_{\mathrm{s}}} = \frac{\bar{\boldsymbol{s}}_L^*}{\|\bar{\boldsymbol{s}}_L\|_2} = \frac{\bar{\boldsymbol{s}}_L^*}{\sqrt{NL\hat{P}_{\mathrm{s}}}}.
\end{aligned}$$

For the MSE expression in (27), we also require $\boldsymbol{P}_{\bar{\boldsymbol{a}}_{\mathrm{SS}}}^{\perp} = \boldsymbol{U}_{\mathrm{SS}_{\mathrm{n}}} \boldsymbol{U}_{\mathrm{SS}_{\mathrm{n}}}^{\mathrm{H}} = \boldsymbol{I}_{M_{\mathrm{sub}}} - \frac{1}{M_{\mathrm{sub}}} \bar{\boldsymbol{a}}_{\mathrm{SS}} \bar{\boldsymbol{a}}_{\mathrm{SS}}^{\mathrm{H}}$, which is the projection matrix onto the noise subspace. Moreover, we have $\boldsymbol{\Phi}^{(r)} = \mathrm{e}^{\mathrm{j}\mu^{(r)}}$ and hence, the eigenvectors are $\boldsymbol{p}_i^{(r)} = \boldsymbol{q}_i^{(r)} = 1$. The SO moments $\boldsymbol{R}_{\mathrm{SS}}$ and $\boldsymbol{C}_{\mathrm{SS}}$ of the noise are given by (29) with $\boldsymbol{R}_{\mathrm{nn}} = \sigma_{\mathrm{n}}^2 \boldsymbol{I}_M$ and $\boldsymbol{C}_{\mathrm{nn}} = \boldsymbol{0}$.

Inserting these expressions into (27), we get

$$\mathbb{E}\left\{ (\Delta\mu^{(r)})^2 \right\} = \frac{1}{2} \cdot \boldsymbol{z}^{\mathrm{H}} \boldsymbol{R}_{\mathrm{SS}}^{\mathrm{T}} \boldsymbol{z} = \frac{1}{2} \cdot \boldsymbol{z}^{\mathrm{T}} \boldsymbol{R}_{\mathrm{SS}} \boldsymbol{z}^* \quad (61)$$

with $\boldsymbol{z} = \boldsymbol{W}_{\mathrm{SS}}^{\mathrm{T}} \boldsymbol{r}_{\mathrm{SS}_i}^{(r)}$ and

$$\boldsymbol{r}_{\mathrm{SS}_i}^{(r)} = \left[\left(\tilde{\boldsymbol{J}}_{\mathrm{SS}_1}^{(r)} \frac{\bar{\boldsymbol{a}}_{\mathrm{SS}}}{\sqrt{M_{\mathrm{sub}}}} \right)^{+} \left(\tilde{\boldsymbol{J}}_{\mathrm{SS}_2}^{(r)} / \mathrm{e}^{\mathrm{j}\mu^{(r)}} - \tilde{\boldsymbol{J}}_{\mathrm{SS}_1}^{(r)} \right) \right]^{\mathrm{T}} \in \mathbb{C}^{M_{\mathrm{sub}} \times 1},$$

$$\boldsymbol{W}_{\mathrm{SS}} = \left(\frac{1}{\sqrt{M_{\mathrm{sub}} NL\hat{P}_{\mathrm{s}}}} \cdot \frac{\bar{\boldsymbol{s}}_L^{\mathrm{H}}}{\sqrt{NL\hat{P}_{\mathrm{s}}}} \right) \otimes \boldsymbol{P}_{\bar{\boldsymbol{a}}_{\mathrm{SS}}}^{\perp} \in \mathbb{C}^{M_{\mathrm{sub}} \times M_{\mathrm{sub}} NL}.$$

Note that the term $\boldsymbol{z}^{\mathrm{T}}$ can also be written as $\boldsymbol{z}^{\mathrm{T}} = \tilde{\boldsymbol{s}}^{\mathrm{T}} \otimes \tilde{\boldsymbol{a}}^{(r)^{\mathrm{T}}}$, where

$$\tilde{\boldsymbol{s}}^{\mathrm{T}} = \frac{1}{\sqrt{M_{\mathrm{sub}} N L \hat{P}_{\mathrm{s}}}} \cdot \frac{(\boldsymbol{a}_L \otimes \bar{\boldsymbol{s}})^{\mathrm{H}}}{\sqrt{N L \hat{P}_{\mathrm{s}}}}, \tag{62}$$

$$\tilde{\boldsymbol{a}}^{(r)^{\mathrm{T}}} = \left(\tilde{\boldsymbol{J}}^{(r)}_{\mathrm{SS}_1} \frac{\bar{\boldsymbol{a}}_{\mathrm{SS}}}{\sqrt{M_{\mathrm{sub}}}} \right)^{+} \left(\tilde{\boldsymbol{J}}^{(r)}_{\mathrm{SS}_2} / \mathrm{e}^{\mathrm{j}\mu^{(r)}} - \tilde{\boldsymbol{J}}^{(r)}_{\mathrm{SS}_1} \right) \boldsymbol{P}^{\perp}_{\bar{\boldsymbol{a}}_{\mathrm{SS}}}. \tag{63}$$

Next, we further simplify the expression $\tilde{\boldsymbol{a}}^{(r)^{\mathrm{T}}}$ and expand the pseudo-inverse of $\tilde{\boldsymbol{J}}^{(r)}_{\mathrm{SS}_1} \bar{\boldsymbol{a}}_{\mathrm{SS}}$ using the relation $\boldsymbol{x}^{+} = \boldsymbol{x}^{\mathrm{H}} / \|\boldsymbol{x}\|_2^2$. As $\tilde{\boldsymbol{J}}^{(r)}_{\mathrm{SS}_1}$ selects $M_{\mathrm{sub}_r} - 1$ out of M_{sub_r} elements in the r-th mode, we have $\|\tilde{\boldsymbol{J}}^{(r)}_{\mathrm{SS}_1} \bar{\boldsymbol{a}}_{\mathrm{SS}}\|_2^2 = \frac{M_{\mathrm{sub}}}{M_{\mathrm{sub}_r}} \cdot (M_{\mathrm{sub}_r} - 1)$. Then, taking the shift invariance equation $\tilde{\boldsymbol{J}}^{(r)}_{\mathrm{SS}_2} \bar{\boldsymbol{a}}_{\mathrm{SS}} / \mathrm{e}^{\mathrm{j}\mu^{(r)}} - \tilde{\boldsymbol{J}}^{(r)}_{\mathrm{SS}_1} \bar{\boldsymbol{a}}_{\mathrm{SS}} = \boldsymbol{0}$ in the r-th mode into account, we obtain

$$\tilde{\boldsymbol{a}}^{(r)^{\mathrm{T}}} = \frac{\sqrt{M_{\mathrm{sub}}} M_{\mathrm{sub}_r}}{M_{\mathrm{sub}} (M_{\mathrm{sub}_r} - 1)} \cdot \breve{\boldsymbol{a}}^{(r)^{\mathrm{T}}}, \tag{64}$$

$$\breve{\boldsymbol{a}}^{(r)^{\mathrm{T}}} = \bar{\boldsymbol{a}}^{\mathrm{H}}_{\mathrm{SS}} \left(\tilde{\boldsymbol{J}}^{(r)^{\mathrm{H}}}{}_{\mathrm{SS}_2} \tilde{\boldsymbol{J}}^{(r)}_{\mathrm{SS}_2} - \tilde{\boldsymbol{J}}^{(r)^{\mathrm{H}}}{}_{\mathrm{SS}_1} \tilde{\boldsymbol{J}}^{(r)}_{\mathrm{SS}_1} \right). \tag{65}$$

Since the vector $\bar{\boldsymbol{a}}_{\mathrm{SS}}$ and the matrices $\tilde{\boldsymbol{J}}^{(r)}_{\mathrm{SS}_k}, k = 1, 2$, contained in $\bar{\boldsymbol{a}}^{(r)^{\mathrm{T}}}$ can be written as $\bar{\boldsymbol{a}}_{\mathrm{SS}} = \bar{\boldsymbol{a}}_1^{(1)} \otimes \cdots \otimes \bar{\boldsymbol{a}}_1^{(R)}$ and $\tilde{\boldsymbol{J}}^{(r)}_{\mathrm{SS}_k} = \boldsymbol{I}_{\prod_{l=1}^{r-1} M_{\mathrm{sub}_l}} \otimes \boldsymbol{J}^{(r)}_{\mathrm{SS}_k} \otimes \boldsymbol{I}_{\prod_{l=r+1}^{R} M_{\mathrm{sub}_l}}$, all the unaffected modes can be factored out of $\breve{\boldsymbol{a}}^{(r)^{\mathrm{T}}}$, yielding

$$\begin{aligned} \breve{\boldsymbol{a}}^{(r)^{\mathrm{T}}} = & \left(\bar{\boldsymbol{a}}_1^{(1)} \otimes \cdots \otimes \bar{\boldsymbol{a}}_1{}^{(r-1)} \right)^{\mathrm{H}} \otimes \breve{\boldsymbol{a}}_1^{(r)^{\mathrm{T}}} \\ & \otimes \left(\bar{\boldsymbol{a}}_1^{(r+1)} \otimes \cdots \otimes \bar{\boldsymbol{a}}_1{}^{(R)} \right)^{\mathrm{H}}, \end{aligned} \tag{66}$$

where we have $\breve{\boldsymbol{a}}_1^{(r)^{\mathrm{T}}} = \bar{\boldsymbol{a}}_1^{(r)^{\mathrm{H}}} (\boldsymbol{J}^{(r)^{\mathrm{H}}}_{\mathrm{SS}_2} \boldsymbol{J}^{(r)}_{\mathrm{SS}_2} - \boldsymbol{J}^{(r)^{\mathrm{H}}}_{\mathrm{SS}_1} \boldsymbol{J}^{(r)}_{\mathrm{SS}_1})$ with $\bar{\boldsymbol{a}}_1^{(r)^{\mathrm{H}}} = [\mathrm{e}^{\mathrm{j}\frac{(M_r-1)}{2}\mu^{(r)}}, \ldots, \mathrm{e}^{-\mathrm{j}\frac{(M_r-2L_r-1)}{2}\mu^{(r)}}, \mathrm{e}^{-\mathrm{j}\frac{(M_r-2L_r+1)}{2}\mu^{(r)}}]$. Then, it is easy to verify that

$$\breve{\boldsymbol{a}}_1^{(r)^{\mathrm{T}}} = \left[-\mathrm{e}^{\mathrm{j}\frac{(M_r-1)}{2}\mu^{(r)}}, 0, \ldots, 0, \mathrm{e}^{-\mathrm{j}\frac{(M_r-2L_r+1)}{2}\mu^{(r)}} \right].$$

Thus, the MSE expression in (61) is given by

$$\mathbb{E}\left\{ (\Delta\mu^{(r)})^2 \right\} = \frac{k^2}{2} \cdot \boldsymbol{v}^{\mathrm{T}} \boldsymbol{R}_{\mathrm{SS}} \boldsymbol{v}^{*}, \tag{67}$$

where we haved used $\boldsymbol{z}^{\mathrm{T}} = k \cdot \boldsymbol{v}^{\mathrm{T}}$ with $\boldsymbol{v}^{\mathrm{T}} = \boldsymbol{a}_L^{\mathrm{H}} \otimes \bar{\boldsymbol{s}}^{\mathrm{H}} \otimes \breve{\boldsymbol{a}}^{(r)^{\mathrm{T}}}$ and $k = \frac{1}{NL\hat{P}_{\mathrm{s}}} \cdot \frac{M_{\mathrm{sub}_r}}{M_{\mathrm{sub}}(M_{\mathrm{sub}_r}-1)}$. After straightforward calculations, we further simplify (67) to obtain (68)–(70) at the bottom of the page, where c_p in (70) is given by (47) and it can be shown that the last term in (69) evaluates to $2 \cdot (L_r - \max\{2 \cdot L_r - M_r, 0\}) = 2 \cdot \min\{L_r, M_r - L_r\}$. Consequently, the MSE of R-D Standard ESPRIT with spatial smoothing is given by

$$\begin{aligned} \mathbb{E}\left\{ (\Delta\mu^{(r)})^2 \right\} &= \frac{\sigma_{\mathrm{n}}^2}{N\hat{P}_{\mathrm{s}}} \cdot \frac{M^2_{\mathrm{sub}_r} \min\{L_r, M_r - L_r\}}{L^2 M^2_{\mathrm{sub}} (M_{\mathrm{sub}_r} - 1)^2} \cdot \prod_{\substack{p=1 \\ p \neq r}}^{R} c_p \\ &= \frac{\sigma_{\mathrm{n}}^2}{N\hat{P}_{\mathrm{s}}} \cdot \frac{\min\{L_r, M_r - L_r\}}{(M_r - L_r)^2 L_r^2} \cdot \prod_{\substack{p=1 \\ p \neq r}}^{R} \frac{c_p}{M^2_{\mathrm{sub}_p} L_p^2}, \end{aligned} \tag{71}$$

where we have used the fact that $M_{\mathrm{sub}} = M_{\mathrm{sub}_r} \cdot \prod_{\substack{p=1 \\ p \neq r}}^{R} M_{\mathrm{sub}_p}$ and $L = L_r \cdot \prod_{\substack{p=1 \\ p \neq r}}^{R} L_p$. Equation (71) is the desired result. ■

B. MSE for R-D Unitary ESPRIT With Spatial Smoothing

The second part of the theorem is to show that for a single source, the MSE of R-D Unitary ESPRIT with spatial smoothing in (31) is the same as the MSE of R-D Standard ESPRIT with spatial smoothing in (27). Firstly, we simplify $\tilde{\boldsymbol{X}}_{\mathrm{SS}_0}$ from (30) and find

$$\begin{aligned} \tilde{\boldsymbol{X}}_{\mathrm{SS}_0} &= \left[\bar{\boldsymbol{a}}_{\mathrm{SS}} \bar{\boldsymbol{s}}_L^{\mathrm{T}},\ \boldsymbol{\Pi}_{M_{\mathrm{sub}}} \bar{\boldsymbol{a}}^{*}_{\mathrm{SS}} \bar{\boldsymbol{s}}_L^{\mathrm{H}} \boldsymbol{\Pi}_{NL} \right] && (72) \\ &= \bar{\boldsymbol{a}}_{\mathrm{SS}} \left[\bar{\boldsymbol{s}}_L^{\mathrm{T}},\ \mathrm{e}^{\mathrm{j}\sum_{r=1}^{R}(L_r-1)\mu^{(r)}} \bar{\boldsymbol{s}}_L^{\mathrm{H}} \boldsymbol{\Pi}_{NL} \right] \\ &= \bar{\boldsymbol{a}}_{\mathrm{SS}} \bar{\bar{\boldsymbol{s}}}_L^{\mathrm{T}}, && (73) \end{aligned}$$

where in (72), we have used the fact that $\boldsymbol{\Pi}_{M_{\mathrm{sub}_r}} \bar{\boldsymbol{a}}_1^{(r)^{*}}(\mu^{(r)}) = \bar{\boldsymbol{a}}_1^{(r)}(\mu^{(r)}) \mathrm{e}^{\mathrm{j}(L_r-1)\mu^{(r)}}$ holds for a ULA in the r-th mode. Moreover, we have defined

$$\bar{\bar{\boldsymbol{s}}}_L = \begin{bmatrix} \bar{\boldsymbol{s}}_L \\ \mathrm{e}^{\mathrm{j}\sum_{r=1}^{R}(L_r-1)\mu^{(r)}} \boldsymbol{\Pi}_{NL} \bar{\boldsymbol{s}}_L^{*} \end{bmatrix} = \begin{bmatrix} \boldsymbol{a}_L \otimes \bar{\boldsymbol{s}} \\ \boldsymbol{a}_L \otimes \boldsymbol{\Pi}_N \bar{\boldsymbol{s}}^{*} \end{bmatrix}. \tag{74}$$

$$\mathbb{E}\left\{ (\Delta\mu^{(r)})^2 \right\} = \frac{k^2}{2} \cdot \sigma_{\mathrm{n}}^2 \cdot \bar{\boldsymbol{s}}^{\mathrm{H}} \bar{\boldsymbol{s}} \cdot \sum_{\underline{\boldsymbol{\ell}}=\underline{\boldsymbol{1}}}^{\underline{\boldsymbol{L}}} \sum_{\underline{\boldsymbol{m}}=\underline{\boldsymbol{1}}}^{\underline{\boldsymbol{L}}} \left(\left(\prod_{\substack{p=1 \\ p \neq r}}^{R} \boldsymbol{a}_1^{(p)^{\mathrm{H}}} \boldsymbol{J}^{(M_p)}_{\ell_p} \boldsymbol{J}^{(M_p)^{\mathrm{T}}}_{m_p} \boldsymbol{a}_1^{(p)} \right) \cdot \breve{\boldsymbol{a}}_1^{(r)^{\mathrm{T}}} \boldsymbol{J}^{(M_r)}_{\ell_r} \boldsymbol{J}^{(M_r)^{\mathrm{T}}}_{m_r} \breve{\boldsymbol{a}}_1^{(r)^{*}} \cdot \mathrm{e}^{\mathrm{j}\sum_{s=1}^{R}\mu^{(s)}(\ell_s - m_s)} \right) \tag{68}$$

$$= \frac{k^2}{2} \cdot \sigma_{\mathrm{n}}^2 \cdot N\hat{P}_{\mathrm{s}} \cdot \left(\prod_{\substack{p=1 \\ p \neq r}}^{R} \boldsymbol{a}_1^{(p)^{\mathrm{H}}} \left(\sum_{\ell_p=1}^{L_p} \sum_{m_p=1}^{L_p} \boldsymbol{J}^{(M_p)}_{\ell_p} \boldsymbol{J}^{(M_p)^{\mathrm{T}}}_{m_p} \right) \boldsymbol{a}_1^{(p)} \right) \cdot \breve{\boldsymbol{a}}_1^{(r)^{\mathrm{T}}} \left(\sum_{\ell_r=1}^{L_r} \sum_{m_r=1}^{L_r} \boldsymbol{J}^{(M_r)}_{\ell_r} \boldsymbol{J}^{(M_r)^{\mathrm{T}}}_{m_r} \cdot \mathrm{e}^{\mathrm{j}\sum_{s=1}^{R}\mu^{(s)}(\ell_s - m_s)} \right) \breve{\boldsymbol{a}}_1^{(r)^{*}} \tag{69}$$

$$= \frac{k^2}{2} \cdot \sigma_{\mathrm{n}}^2 \cdot N\hat{P}_{\mathrm{s}} \cdot \left(\prod_{\substack{p=1 \\ p \neq r}}^{R} c_p \right) \cdot 2 \cdot \min\{L_r, M_r - L_r\} \tag{70}$$

Note that $\|\bar{\tilde{\boldsymbol{s}}}_L\|_2^2 = 2NL\hat{P}_{\mathrm{s}}$. The subspaces from the SVD of $\tilde{\boldsymbol{X}}_{\mathrm{SS}_0}$ are obtained as

$$\tilde{\boldsymbol{u}}_{\mathrm{SS}_{\mathrm{s}}} = \frac{\bar{\boldsymbol{a}}_{\mathrm{SS}}}{\sqrt{M_{\mathrm{sub}}}} = \boldsymbol{u}_{\mathrm{SS}_{\mathrm{s}}}, \quad \tilde{\sigma}_{\mathrm{SS}_{\mathrm{s}}} = \sqrt{2M_{\mathrm{sub}}NL\hat{P}_{\mathrm{s}}},$$
$$\tilde{\boldsymbol{v}}_{\mathrm{SS}_{\mathrm{s}}} = \frac{\bar{\tilde{\boldsymbol{s}}}_L^*}{\sqrt{2NL\hat{P}_{\mathrm{s}}}}.$$

Compared to the previous subsection, it is apparent that FBA does not affect the column space $\boldsymbol{u}_{\mathrm{SS}_{\mathrm{s}}}$, such that $\tilde{\boldsymbol{U}}_{\mathrm{SS}_{\mathrm{n}}} = \boldsymbol{U}_{\mathrm{SS}_{\mathrm{n}}}$ and thus $\tilde{\boldsymbol{P}}^{\perp}_{\bar{\boldsymbol{a}}_{\mathrm{SS}}} = \boldsymbol{P}^{\perp}_{\bar{\boldsymbol{a}}_{\mathrm{SS}}}$. However, FBA destroys the circular symmetry of the noise, resulting in an additional term in the MSE expression. Following the derivation for R-D Standard ESPRIT with spatial smoothing, it can be shown that $\tilde{\boldsymbol{z}}^{\mathrm{T}} = \tilde{\boldsymbol{r}}_{\mathrm{SS}_i}^{(r)^{\mathrm{T}}} \tilde{\boldsymbol{W}}_{\mathrm{SS}} = \tilde{\tilde{\boldsymbol{s}}}^{\mathrm{T}} \otimes \tilde{\boldsymbol{a}}^{(r)^{\mathrm{T}}}$, where

$$\tilde{\tilde{\boldsymbol{s}}}^{\mathrm{T}} = \frac{1}{\sqrt{2M_{\mathrm{sub}}NL\hat{P}_{\mathrm{s}}}} \cdot \frac{\bar{\tilde{\boldsymbol{s}}}_L^{\mathrm{H}}}{\sqrt{2NL\hat{P}_{\mathrm{s}}}} \tag{75}$$

and $\tilde{\boldsymbol{a}}^{(r)^{\mathrm{T}}}$ is given as in (63). Thus, the MSE expression for R-D Unitary ESPRIT with spatial smoothing in (31) can be written as

$$\mathbb{E}\left\{(\Delta\mu^{(r)})^2\right\} = \frac{1}{2} \cdot \left(\tilde{\boldsymbol{z}}^{\mathrm{T}} \tilde{\boldsymbol{R}}_{\mathrm{SS}} \tilde{\boldsymbol{z}}^* - \mathrm{Re}\left\{\tilde{\boldsymbol{z}}^{\mathrm{T}} \tilde{\boldsymbol{C}}_{\mathrm{SS}} \tilde{\boldsymbol{z}}\right\}\right), \tag{76}$$

where $\tilde{\boldsymbol{R}}_{\mathrm{SS}} = \boldsymbol{I}_2 \otimes \boldsymbol{R}_{\mathrm{SS}}$ and $\tilde{\boldsymbol{C}}_{\mathrm{SS}} = \boldsymbol{\Pi}_2 \otimes (\boldsymbol{\Pi}_{M_{\mathrm{sub}}NL} \boldsymbol{R}_{\mathrm{SS}})$. Expanding (76), we have

$$\mathbb{E}\left\{(\Delta\mu^{(r)})^2\right\} = \frac{\tilde{k}^2}{2} \cdot \left(\boldsymbol{v}^{\mathrm{T}} \boldsymbol{R}_{\mathrm{SS}} \boldsymbol{v}^* + \bar{\boldsymbol{v}}^{\mathrm{T}} \boldsymbol{R}_{\mathrm{SS}} \bar{\boldsymbol{v}}^*\right.$$
$$\left. - \mathrm{Re}\left\{\boldsymbol{v}^{\mathrm{T}} \boldsymbol{\Pi}_{M_{\mathrm{sub}}NL} \boldsymbol{R}_{\mathrm{SS}} \bar{\boldsymbol{v}} + \bar{\boldsymbol{v}}^{\mathrm{T}} \boldsymbol{\Pi}_{M_{\mathrm{sub}}NL} \boldsymbol{R}_{\mathrm{SS}} \boldsymbol{v}^*\right\}\right), \tag{77}$$

where $\tilde{\boldsymbol{z}}^{\mathrm{T}} = \tilde{k} \cdot \tilde{\boldsymbol{v}}^{\mathrm{T}}$ with $\tilde{\boldsymbol{v}}^{\mathrm{T}} = [\boldsymbol{v}^{\mathrm{T}}, \bar{\boldsymbol{v}}^{\mathrm{T}}]$, $\bar{\boldsymbol{v}}^{\mathrm{T}} = \boldsymbol{a}_L^{\mathrm{H}} \otimes \bar{\boldsymbol{s}}^{\mathrm{T}} \boldsymbol{\Pi}_N \otimes \check{\boldsymbol{a}}^{(r)^{\mathrm{T}}}$, and $\tilde{k} = \frac{1}{2NL\hat{P}_{\mathrm{s}}} \cdot \frac{M_{\mathrm{sub}_r}}{M_{\mathrm{sub}}(M_{\mathrm{sub}_r}-1)}$. Note that the first term of (77) was already computed in (70) as $2 \cdot \sigma_{\mathrm{n}}^2 \cdot N\hat{P}_{\mathrm{s}} \cdot (\prod_{\substack{p=1 \\ p\neq r}}^{R} c_p) \cdot \min\{L_r, M_r - L_r\}$. The remaining terms can be computed accordingly, where for the second term, we also obtain $2 \cdot \sigma_{\mathrm{n}}^2 \cdot N\hat{P}_{\mathrm{s}} \cdot (\prod_{\substack{p=1 \\ p\neq r}}^{R} c_p) \cdot \min\{L_r, M_r - L_r\}$ while the third and fourth terms both evaluate to $-2 \cdot \sigma_{\mathrm{n}}^2 \cdot N\hat{P}_{\mathrm{s}} \cdot (\prod_{\substack{p=1 \\ p\neq r}}^{R} c_p) \cdot \min\{L_r, M_r - L_r\}$. Inserting these intermediate results into (77), we obtain for the MSE of R-D Unitary ESPRIT with spatial smoothing

$$\mathbb{E}\left\{(\Delta\mu^{(r)})^2\right\} = \frac{\sigma_{\mathrm{n}}^2}{N\hat{P}_{\mathrm{s}}} \cdot \frac{\min\{L_r, M_r - L_r\}}{(M_r - L_r)^2 L_r^2} \cdot \prod_{\substack{p=1 \\ p\neq r}}^{R} \frac{c_p}{M_{\mathrm{sub}_p}^2 L_p^2}, \tag{78}$$

which is equal to (71) and hence proves this part.

C. MSE for R-D NC Standard ESPRIT and R-D NC Unitary ESPRIT with Spatial Smoothing

The third part of the theorem is to show that the MSE of the spatially smoothed versions of R-D NC Standard ESPRIT and R-D NC Unitary ESPRIT is the same as the MSE for R-D Standard ESPRIT and Unitary ESPRIT. As we have already proven that the performance of R-D NC Standard and R-D NC Unitary ESPRIT with spatial smoothing is identical in the high effective SNR in general, this must also hold true for the case $d = 1$. Hence, it is sufficient to simplify the MSE of R-D NC Standard ESPRIT in (40) for this special case. We start by writing $\boldsymbol{X}_{\mathrm{SS}_0}^{(\mathrm{nc})}$ in (22) as

$$\boldsymbol{X}_{\mathrm{SS}_0} = \bar{\boldsymbol{a}}_{\mathrm{SS}}^{(\mathrm{nc})} \bar{\boldsymbol{s}}_L^{\mathrm{T}}, \tag{79}$$

where $\bar{\boldsymbol{s}}_L$ was defined in (60) and $\bar{\boldsymbol{a}}_{\mathrm{SS}}^{(\mathrm{nc})} = [1, \tilde{\Psi}]^{\mathrm{T}} \otimes \bar{\boldsymbol{a}}_{\mathrm{SS}}$ with $\tilde{\Psi} = \Xi^* \Xi^* = \mathrm{e}^{-\mathrm{j}2(\varphi+\delta)}$. This follows from (22) and the fact that $\bar{\boldsymbol{a}}^{(\mathrm{nc})} = [1, \tilde{\Psi}]^{\mathrm{T}} \otimes \bar{\boldsymbol{a}}$ for a uniform R-D array whose phase reference is at the centroid, i.e. $\boldsymbol{\Pi}_M \bar{\boldsymbol{a}}^* = \bar{\boldsymbol{a}}$ holds. Therefore, we have $\|\bar{\boldsymbol{a}}_{\mathrm{SS}}^{(\mathrm{nc})}\|_2^2 = 2M_{\mathrm{sub}}$. The selection matrices $\tilde{\boldsymbol{J}}_{\mathrm{SS}_k}^{(\mathrm{nc})(r)}, k = 1, 2$ are given by $\tilde{\boldsymbol{J}}_{\mathrm{SS}_k}^{(\mathrm{nc})(r)} = \boldsymbol{I}_2 \otimes \tilde{\boldsymbol{J}}_{\mathrm{SS}_k}^{(r)}$. The SVD of (79) can be explicitly expressed as

$$\boldsymbol{u}_{\mathrm{SS}_{\mathrm{s}}}^{(\mathrm{nc})} = \frac{\bar{\boldsymbol{a}}_{\mathrm{SS}}^{(\mathrm{nc})}}{\sqrt{2M_{\mathrm{sub}}}}, \quad \sigma_{\mathrm{SS}_{\mathrm{s}}}^{(\mathrm{nc})} = \sqrt{2M_{\mathrm{sub}}NL\hat{P}_{\mathrm{s}}},$$
$$\boldsymbol{v}_{\mathrm{SS}_{\mathrm{s}}}^{(\mathrm{nc})} = \frac{\bar{\boldsymbol{s}}_L^*}{\sqrt{NL\hat{P}_{\mathrm{s}}}} = \boldsymbol{v}_{\mathrm{SS}_{\mathrm{s}}}.$$

It is evident that the NC preprocessing only affects the column space $\boldsymbol{u}_{\mathrm{SS}_{\mathrm{s}}}^{(\mathrm{nc})}$ while the row space $\boldsymbol{v}_{\mathrm{SS}_{\mathrm{s}}}$ of R-D Standard ESPRIT remains unaffected. Therefore, we have $\boldsymbol{P}^{\perp}_{\bar{\boldsymbol{a}}_{\mathrm{SS}}^{(\mathrm{nc})}} = \boldsymbol{U}_{\mathrm{SS}_{\mathrm{n}}}^{(\mathrm{nc})} \boldsymbol{U}_{\mathrm{SS}_{\mathrm{n}}}^{(\mathrm{nc})^{\mathrm{H}}} = \boldsymbol{I}_{M_{\mathrm{sub}}} - \frac{1}{M_{\mathrm{sub}}} \bar{\boldsymbol{a}}_{\mathrm{SS}}^{(\mathrm{nc})} \bar{\boldsymbol{a}}_{\mathrm{SS}}^{(\mathrm{nc})^{\mathrm{H}}}$. Similarly to FBA, the circular symmetry of the noise is destroyed by the NC preprocessing step. In the NC case, it can be shown that $\boldsymbol{z}^{(\mathrm{nc})^{\mathrm{T}}} = \boldsymbol{r}_{\mathrm{SS}_i}^{(\mathrm{nc})(r)^{\mathrm{T}}} \boldsymbol{W}_{\mathrm{SS}}^{(\mathrm{nc})} = \tilde{\boldsymbol{s}}^{(\mathrm{nc})^{\mathrm{T}}} \otimes \tilde{\boldsymbol{a}}^{(\mathrm{nc})(r)^{\mathrm{T}}}$, where

$$\tilde{\boldsymbol{s}}^{(\mathrm{nc})^{\mathrm{T}}} = \frac{1}{\sqrt{2M_{\mathrm{sub}}NL\hat{P}_{\mathrm{s}}}} \cdot \frac{(\boldsymbol{a}_L \otimes \bar{\boldsymbol{s}})^{\mathrm{H}}}{\sqrt{NL\hat{P}_{\mathrm{s}}}} \tag{80}$$

$$\tilde{\boldsymbol{a}}^{(\mathrm{nc})(r)^{\mathrm{T}}} = \left(\tilde{\boldsymbol{J}}_{\mathrm{SS}_1}^{(\mathrm{nc})(r)} \frac{\bar{\boldsymbol{a}}_{\mathrm{SS}}^{(\mathrm{nc})}}{\sqrt{2M_{\mathrm{sub}}}}\right)^+ \cdot \left(\tilde{\boldsymbol{J}}_{\mathrm{SS}_2}^{(\mathrm{nc})(r)} / \mathrm{e}^{\mathrm{j}\mu^{(r)}} - \tilde{\boldsymbol{J}}_{\mathrm{SS}_1}^{(\mathrm{nc})(r)}\right) \boldsymbol{P}^{\perp}_{\bar{\boldsymbol{a}}_{\mathrm{SS}}^{(\mathrm{nc})}}. \tag{81}$$

Following the lines of the derivation of R-D Standard ESPRIT with spatial smoothing, $\tilde{\boldsymbol{a}}^{(\mathrm{nc})(r)^{\mathrm{T}}}$ can be simplified as

$$\tilde{\boldsymbol{a}}^{(\mathrm{nc})(r)^{\mathrm{T}}} = \frac{\sqrt{2M_{\mathrm{sub}}} M_{\mathrm{sub}_r}}{2M_{\mathrm{sub}}(M_{\mathrm{sub}_r} - 1)} \cdot \begin{bmatrix} 1 \\ \tilde{\Psi} \end{bmatrix}^{\mathrm{H}} \otimes \check{\boldsymbol{a}}^{(r)^{\mathrm{T}}}, \tag{82}$$

where $\bar{\boldsymbol{a}}^{(r)^{\mathrm{T}}}$ is given in (66). Consequently, the MSE for R-D NC Standard ESPRIT with spatial smoothing in (40) can be written as

$$\mathbb{E}\left\{(\Delta\mu^{(r)})^2\right\} = \frac{1}{2} \cdot \left(\boldsymbol{z}^{(\mathrm{nc})^{\mathrm{T}}} \boldsymbol{R}_{\mathrm{SS}}^{(\mathrm{nc})} \boldsymbol{z}^{(\mathrm{nc})^*} - \mathrm{Re}\left\{\boldsymbol{z}^{(\mathrm{nc})^{\mathrm{T}}} \boldsymbol{C}_{\mathrm{SS}}^{(\mathrm{nc})} \boldsymbol{z}\right\}\right), \tag{83}$$

where $\boldsymbol{R}_{\mathrm{SS}}^{(\mathrm{nc})}$ and $\boldsymbol{C}_{\mathrm{SS}}^{(\mathrm{nc})}$ are given according to (43). Next, we use (80) and (82) to express (83) as

$$\mathbb{E}\left\{(\Delta\mu^{(r)})^2\right\} = \frac{{k^{(\mathrm{nc})}}^2}{2} \cdot \left(\boldsymbol{v}^{(\mathrm{nc})^{\mathrm{T}}} \boldsymbol{R}_{\mathrm{SS}}^{(\mathrm{nc})} \boldsymbol{v}^{(\mathrm{nc})^*} - \mathrm{Re}\left\{\boldsymbol{v}^{(\mathrm{nc})^{\mathrm{T}}} \boldsymbol{C}_{\mathrm{SS}}^{(\mathrm{nc})} \boldsymbol{v}^{(\mathrm{nc})}\right\}\right), \tag{84}$$

where again $\boldsymbol{z}^{(\mathrm{nc})^{\mathrm{T}}} = k^{(\mathrm{nc})} \cdot \boldsymbol{v}^{(\mathrm{nc})^{\mathrm{T}}}$ with $\boldsymbol{v}^{(\mathrm{nc})^{\mathrm{T}}} = \boldsymbol{a}_L^{\mathrm{H}} \otimes \bar{\boldsymbol{s}}^{\mathrm{H}} \otimes [\frac{1}{\breve{\Psi}}]^{\mathrm{H}} \otimes \breve{\boldsymbol{a}}^{(r)^{\mathrm{T}}}$ and $k^{(\mathrm{nc})} = \frac{1}{2NL\hat{P}_{\mathrm{s}}} \cdot \frac{M_{\mathrm{sub}_r}}{M_{\mathrm{sub}}(M_{\mathrm{sub}_r}-1)}$. Considering the first term of (84) and expanding $\boldsymbol{R}_{\mathrm{SS}}^{(\mathrm{nc})}$, we apply the same steps as in (68) and (70). As a result, the first term reduces to $4 \cdot \sigma_{\mathrm{n}}^2 \cdot N\hat{P}_{\mathrm{s}} \cdot (\prod_{\substack{p=1 \\ p\neq r}}^{R} c_p) \cdot \min\{L_r, M_r - L_r\}$. The second term of (84) can be computed accordingly to obtain $-4 \cdot \sigma_{\mathrm{n}}^2 \cdot N\hat{P}_{\mathrm{s}} \cdot (\prod_{\substack{p=1 \\ p\neq r}}^{R} c_p) \cdot \min\{L_r, M_r - L_r\}$.

Using these expressions in (84), the MSE of R-D NC Standard ESPRIT with spatial smoothing is given by

$$\mathbb{E}\left\{(\Delta\mu^{(r)})^2\right\} = \frac{\sigma_{\mathrm{n}}^2}{N\hat{P}_{\mathrm{s}}} \cdot \frac{\min\{L_r, M_r - L_r\}}{(M_r - L_r)^2 L_r^2} \cdot \prod_{\substack{p=1 \\ p\neq r}}^{R} \frac{c_p}{M_{\mathrm{sub}_p}^2 L_p^2}. \tag{85}$$

As this result is equal to (71) and (78), the theorem has been proven. ■

Appendix C Proof of Equation (49)

For the proof, we consider the case $L_r \leq \frac{M_r}{2}$, however, the derivation for $L_r > \frac{M_r}{2}$ follows the same steps. The MSE in (46) is given by

$$\mathrm{MSE}_{\mathrm{SS}}^{(r)} \approx \frac{1}{\hat{\rho}} \cdot \frac{a}{(M_r - L_r)^2 L_r} \quad \text{for} \quad L_r \leq \frac{M_r}{2}, \tag{86}$$

where we have defined $a = \prod_{\substack{p=1 \\ p\neq r}}^{R} \frac{c_p}{M_{\mathrm{sub}_p}^2 L_p^2}$. In order to determine the optimal number of subarrays L_r in the r-th mode, we minimize (46) with respect to L_r. That is, we first compute the derivative of (46) with respect to L_r given by

$$\frac{\partial \mathrm{MSE}_{\mathrm{SS}}^{(r)}}{\partial L_r} = \frac{1}{\hat{\rho}} \cdot \frac{a(M_r - 3L_r)}{(L_r - M_r)^3 L_r^2} \tag{87}$$

and then equate (87) to zero and solve for L_r, yielding

$$L_r^{\mathrm{opt}} = \frac{1}{3} \cdot M_r, \tag{88}$$

which is the desired result in (49). ■

References

[1] J. Steinwandt, F. Roemer, and M. Haardt, "Asymptotic performance analysis of ESPRIT-type algorithms for circular and strictly non-circular sources with spatial smoothing," in *Proc. IEEE Int. Conf. Acoust., Speech, Signal Process.*, Florence, Italy, May 2014, pp. 2277–2281.

[2] D. Nion and N. D. Sidiropoulos, "Tensor algebra and multidimensional harmonic retrieval in signal processing for mimo radar," *IEEE Trans. Signal Process.*, vol. 58, no. 11, pp. 5693–5705, Nov. 2010.

[3] H. Cox, "Fundamentals of bistatic active sonar," in *Proceedings of NATO Advanced Study Institute on Underwater Acoustic Data Processing*, Y. T. Chan, Ed. Norwood, MA, USA: Kluwer, 1989.

[4] M. Haardt, R. S. Thomä, and A. Richter, "Multidimensional high-resolution parameter estimation with applications to channel sounding," in *High-Resolution and Robust Signal Processing*, Y. Hua, A. Gershman, and Q. Chen, Eds. New York, NY, USA: Marcel Dekker, 2004, pp. 255–338.

[5] X. Liu, N. D. Sidiropoulos, and T. Jiang, "Multidimensional harmonic retrieval with applications in mimo wireless channel sounding," in *Space-Time Processing for MIMO Communications*, A. Gershman and N. Sidiropoulos, Eds. New York, NY, USA: Wiley, 2005, pp. 41–75.

[6] M. Pesavento, C. F. Mecklenbräuker, and J. F. Böhme, "Multidimensional rank reduction estimator for parametric MIMO channel models," *EURASIP J. Appl. Signal Process.*, vol. 2004, no. 9, pp. 1354–1363, Sep. 2004.

[7] M. Haardt and J. A. Nossek, "Simultaneous Schur decomposition of several non-symmetric matrices to achieve automatic pairing in multidimensional harmonic retrieval problems," *IEEE Trans. Signal Process.*, vol. 46, no. 1, pp. 161–169, Jan. 1998.

[8] B. D. Rao and K. V. S. Hari, "Performance analysis of ESPRIT and TAM in determining the direction of arrival of plane waves in noise," *IEEE Trans. Acoust., Speech, Signal Process.*, vol. 37, no. 12, pp. 1990–1995, Dec. 1989.

[9] F. Li, H. Liu, and R. J. Vaccaro, "Performance analysis for DOA estimation algorithms: Unification, simplifications, and observations," *IEEE Trans. Aerosp. Electron. Syst.*, vol. 29, no. 4, pp. 1170–1184, Oct. 1993.

[10] F. Roemer and M. Haardt, "A framework for the analytical performance assessment of matrix and tensor-based ESPRIT-type algorithms," arXiv:1209.3253, Sep. 2012.

[11] F. Roemer, M. Haardt, and G. Del Galdo, "Analytical performance assessment of multi-dimensional matrix- and tensor-based ESPRIT-type algorithms," *IEEE Trans. Signal Process.*, vol. 62, no. 10, pp. 2611–2625, May 2014.

[12] P. J. Schreier and L. L. Scharf, *Statistical Signal Processing of Complex-Valued Data: The Theory of Improper and Noncircular Signals*, Cambridge, U.K.: Cambridge Univ. Press, 2010.

[13] H. Abeida and J. P. Delmas, "MUSIC-like estimation of direction of arrival for noncircular sources," *IEEE Trans. Signal Process.*, vol. 54, no. 7, pp. 2678–2690, Jul. 2006.

[14] A. Ferreol and P. Chevalier, "Higher order direction finding for arbitrary noncircular sources: The NC-2q-MUSIC algorithm," in *Proc. Eur. Signal Process. Conf.*, Aalborg, Denmark, Aug. 2010, pp. 671–675.

[15] A. Ferreol and P. Chevalier, "New insights into second and fourth-order direction finding for non-circular sources," in *Proc. IEEE Sensor Array Multichannel Signal Process. Workshop*, A Coruña, Spain, 2014, pp. 465–468.

[16] P. Chargé, Y. Wang, and J. Saillard, "A non-circular sources direction finding method using polynomial rooting," *Signal Process.*, vol. 81, no. 8, pp. 1765–1770, Aug. 2001.

[17] A. Zoubir, P. Chargé, and Y. Wang, "Non circular sources localization with ESPRIT," in *Proc. Eur. Conf. Wireless Technol.*, Munich, Germany, Oct. 2003, pp. 297–300.

[18] M. Haardt and F. Roemer, "Enhancements of Unitary ESPRIT for non-circular sources," in *Proc. IEEE Int. Conf. Acoust., Speech, Signal Process.*, Montreal, Canada, May 2004, pp. 101–104.

[19] J. Steinwandt, F. Roemer, M. Haardt, and G. Del Galdo, "R-dimensional ESPRIT-type algorithms for strictly second-order non-circular sources and their performance analysis," *IEEE Trans. Signal Process.*, vol. 62, no. 18, pp. 4824–4838, Sep. 2014.

[20] H. Abeida and J. P. Delmas, "Statistical performance of MUSIC-like algorithms in resolving noncircular sources," *IEEE Trans. Signal Process.*, vol. 56, no. 9, pp. 4317–4329, Sep. 2008.

[21] F. Gao, A. Nallanathan, and Y. Wang, "Improved music under the coexistence of both circular and noncircular sources," *IEEE Trans. Signal Process.*, vol. 56, no. 7, pp. 3033–3038, Jul. 2008.

[22] J. Steinwandt, F. Roemer, and M. Haardt, "ESPRIT-type algorithms for a received mixture of circular and strictly non-circular signals," in *Proc. IEEE Int. Conf. Acoust., Speech, Signal Process.*, Brisbane, Australia, Apr. 2015, pp. 2809–2813.

[23] J. Steinwandt, F. Roemer, and M. Haardt, "Analytical performance assessment of ESPRIT-type algorithms for coexisting circular and strictly non-circular signals," in *Proc. IEEE Int. Conf. Acoust., Speech, Signal Process.*, Shanghai, China, Mar. 2016, pp. 2931–2935.

[24] M. Haardt, *Efficient One-, Two-, and Multidimensional High-Resolution Array Signal Processing*. Aachen, Germany: Shaker Verlag, 1997.

[25] D. Tse and P. Viswanath, *Fundamentals of Wireless Communications*. Cambridge, U.K.: Cambridge Univ. Press, 2005.

[26] P. Pal and P. P. Vaidyanathan, "Nested arrays: A novel approach to array processing with enhanced degrees of freedom," *IEEE Trans. Signal Process.*, vol. 58, no. 8, pp. 4167–4181, Aug. 2010.

[27] P. Comon and G. H. Golub, "Tracking a few extreme singular values and vectors in signal processing," *Proc. IEEE*, vol. 78, no. 8, pp. 1327–1343, Aug. 1990.

[28] J. E. Evans, J. R. Johnson, and D. F. Sun, "Application of advanced signal processing techniques to angle of arrival estimation in atc navigation and surveillance systems," MIT Lincoln Lab., Lexington, MA, USA, Tech. Rep. 582, 1982.

[29] T.-J. Shan, M. Wax, and T. Kailath, "On spatial smoothing for direction-of-arrival estimation of coherent signals," *IEEE Trans. Acoust., Speech, Signal Process.*, vol. 33, no. 4, pp. 806–811, Aug. 1985.

[30] S. U. Pillai and B. H. Kwon, "Forward/backward spatial smoothing techniques for coherent signal identification," *IEEE Trans. Acoust., Speech, Signal Process.*, vol. 37, no. 1, pp. 8–15, Jan. 1989.
[31] S. U. Pillai and B. H. Kwon, "Performance analysis of MUSIC-type high resolution estimators for direction finding in correlated and coherent scenes," *IEEE Trans. Acoust., Speech, Signal Process.*, vol. 37, no. 8, pp. 1176–1189, Aug. 1989.
[32] B. D. Rao and K. V. S. Hari, "Effect of spatial smoothing on the performance of MUSIC and minimum-norm method," *Proc. Inst. Elect. Eng. F*, vol. 137, pp. 449–458, Dec. 1990.
[33] B. D. Rao and K. V. S. Hari, "Weighted subspace methods and spatial smoothing: Analysis and comparison," *IEEE Trans. Signal Process.*, vol. 41, no. 2, pp. 788–803, Feb. 1993.
[34] Y. Hua and T. K. Sarkar, "Matrix pencil method for estimating parameters of exponentially damped/undamped sinusoids in noise," *IEEE Trans. Signal Process.*, vol. 38, no. 5, pp. 814–824, May 1990.
[35] K. V. S. Hari and B. V. Ramakrishnan, "Performance analysis of modified spatial smoothing technique for direction estimation," *Signal Process.*, vol. 79, pp. 73–85, Nov. 1999.
[36] A. N. Lemma, A.-J. van der Veen, and E. F. Deprettere, "Analysis of joint angle-frequency estimation using ESPRIT," *IEEE Trans. Signal Process.*, vol. 51, no. 5, pp. 1264–1283, May 2003.
[37] A. J. Weiss and B. Friedlander, "Performance analysis of spatial smoothing with interpolated data," *IEEE Trans. Signal Process.*, vol. 41, no. 5, pp. 1881–1892, May 1993.
[38] J. Steinwandt, F. Roemer, M. Haardt, and G. Del Galdo, "Deterministic Cramér-Rao bound for strictly non-circular sources and analytical analysis of the achievable gains," *IEEE Trans. Signal Process.*, vol. 64, no. 17, pp. 4417–4431, Sep. 2016.
[39] T. Fu and X. Gao, "Simultaneous diagonalization with similarity transformation for non-defective matrices," in *Proc. IEEE Int. Conf. Acoust., Speech, Signal Process.*, Toulouse, France, May 2006, p. IV.
[40] J. R. Magnus and H. Neudecker, *Matrix Differential Calculus With Applications in Statistics and Econometrics*. Hoboken, NJ, USA: Wiley, 1995.

Jens Steinwandt (S'11) received the B.Sc. and M.Sc. degrees in electrical and communications engineering from Ilmenau University of Technology, Ilmenau, Germany, in August 2009 and July 2011, respectively. Since August 2011, he has been a Research Assistant in the Communications Research Laboratory, Ilmenau University of Technology. From May 2010 to March 2011 and from October 2013 to December 2013, he was a Visiting Research Assistant in the Communications Group, Department of Electronics, University of York, York, U.K. and the Department of Signal Processing and Acoustics, Aalto University, Helsinki, Finland, respectively. His research interests include high-resolution parameter estimation, MIMO communications, optimization theory, and compressed sensing. Mr. Steinwandt received the Best Master's Thesis Award from the Förder- und Freundeskreis (FFK) of the Ilmenau University of Technology in 2011.

Florian Roemer (S'04–M'13–SM'16) studied computer engineering at the Ilmenau University of Technology, Germany and McMaster University, Hamilton, ON, Canada. He received the Diplom-Ingenieur degree in communications engineering and the doctoral (Dr.-Ing.) degree in electrical engineering from the Ilmenau University of Technology, Ilmenau, Germany, in October 2006 and October 2012, respectively. From December 2006 to September 2012, he has been a Research Assistant in the Communications Research Laboratory, Ilmenau University of Technology. In October 2012, he has joined the Digital Broadcasting Research Group, a joint research activity between the Fraunhofer Institute for Integrated Circuits IIS and Ilmenau University of Technology, as a Postdoctoral Research Fellow. His research interests include multi-dimensional signal processing, high-resolution parameter estimation, MIMO communications as well as compressive sensing. Mr. Roemer, for his diploma thesis, received the Siemens Communications Academic Award in 2006 and for his dissertation he received the Best Dissertation Award from the Förder- und Freundeskreis, Ilmenau University of Technology in 2013 as well as the EURASIP Best Dissertation Award in 2016. He has also served as a Member of the organizing committee of the 19th International Workshop on Smart Antennas 2015 at Ilmenau, Germany.

Martin Haardt (S'90–M'98–SM'99) studied electrical engineering at the Ruhr-University Bochum, Germany, and at Purdue University, USA, and received the Diplom-Ingenieur (M.S.) degree from the Ruhr-University Bochum, Bochum, Germany, in 1991 and the Doktor-Ingenieur (Ph.D.) degree from Munich University of Technology, Munich, Germany, in 1996. In 1997, he joined Siemens Mobile Networks, Munich, Germany, where he was responsible for strategic research for third generation mobile radio systems. From 1998 to 2001, he was the Director for International Projects and University Cooperations in the mobile infrastructure business of Siemens in Munich, where his work focused on mobile communications beyond the third generation. During his time at Siemens, he also taught in the international Master of Science in Communications Engineering program at Munich University of Technology. Since 2001, he has been a Full Professor in the Department of Electrical Engineering and Information Technology and the Head of the Communications Research Laboratory, Ilmenau University of Technology, Germany. Since 2012, he has been serving as an Honorary Visiting Professor in the Department of Electronics, University of York, York, U.K. His research interests include wireless communications, array signal processing, high-resolution parameter estimation, as well as numerical linear and multi-linear algebra. He has received the 2009 Best Paper Award from the IEEE Signal Processing Society, the Vodafone (formerly Mannesmann Mobilfunk) Innovations-Award for outstanding research in mobile communications, the ITG Best Paper Award from the Association of Electrical Engineering, Electronics, and Information Technology (VDE), and the Rohde & Schwarz Outstanding Dissertation Award. In the fall of 2006 and the fall of 2007, he was a Visiting Professor at the University of Nice, Sophia-Antipolis, France and the University of York, U.K., respectively. Dr. Haardt has served as an Associate Editor for the IEEE TRANSACTIONS ON SIGNAL PROCESSING (2002–2006 and since 2011), the IEEE SIGNAL PROCESSING LETTERS (2006–2010), the *Research Letters in Signal Processing* (2007–2009), the Hindawi *Journal of Electrical and Computer Engineering* (since 2009), the *EURASIP Signal Processing Journal* (since 2011), and as a Guest Editor for the *EURASIP Journal on Wireless Communications and Networking*. He has also served as an Elected Member of the Sensor Array and Multichannel (SAM) technical committee of the IEEE Signal Processing Society (since 2011), as the technical Co-chair of the IEEE International Symposiums on Personal Indoor and Mobile Radio Communications 2005 in Berlin, Germany, as the Technical Program Chair of the IEEE International Symposium on Wireless Communication Systems (ISWCS) 2010 in York, U.K., as the General Chair of ISWCS 2013 in Ilmenau, Germany, and as the General Co-chair of the 5th IEEE International Workshop on Computational Advances in Multi-Sensor Adaptive Processing 2013 in Saint Martin, French Caribbean, the 19th International Workshop on Smart Antennas 2015 in Ilmenau, as well as the 9th IEEE SAM Signal Processing Workshop 2016 in Rio de Janeiro, Brazil.

Giovanni Del Galdo (M'12) was born in Merano, Italy, in 1977. He studied telecommunications engineering at the Politecnico di Milano and received the Master's degree in 2002. He then joined the Communications Research Laboratory, Ilmenau University of Technology (TUIL), Ilmenau, Germany, where he received the Doctoral degree in 2007 on the topic of channel modeling for MIMO wireless communication systems. Shortly thereafter, he joined the Fraunhofer Institute for Integrated Circuits IIS and the International Audio Laboratories Erlangen as a Senior Scientist, where he worked on audio watermarking, parametric representations of spatial sound, and sound field analysis via microphone arrays.

In 2012, he was appointed as a Full Professor in the Department of Electrical Engineering and Information Technology, TUIL and the Head of the DVT Research Group, a joint activity between TUIL and Fraunhofer IIS on the research area of wireless distribution systems and digital broadcasting. The group manages and develops the Fraunhofer IIS Facility for Over-the-air Research and Testing further. His research interests include the analysis, modeling, and manipulation of multidimensional signals, over-the-air testing for terrestrial and satellite communication systems, and sparsity promoting reconstruction methods.